Sensor and Simulation Notes
Note 215

TRANSIENT RADIATED FIELDS FROM SOURCES LOCATED ON A PLANAR SURFACE

The Dikewood Corporation
Albuquerque, NM 87106

January 1977

Final Report

Approved for public release; distribution unlimited.

AIR FORCE WEAPONS LABORATORY
Air Force Systems Command
Kirtland Air Force Base, NM 87117

PL 96-1005

Transient Radiated Fields from Sources Located
on a Planar Surface

Charles E. Smith
Electrical Engineering Department
The University of Mississippi

Abstract

Expressions for the transient radiated electric fields of a planar
array of sources are developed for elements having known field distribu-
tion, as well as time delay, located on an infinite, perfectly-conducting,
ground plane. The analysis of such arrays is based on a Green's function
approach to the electric vector potential problem. Planar arrays of two-
dimensional sources are analyzed in this manner using numerical compu-
tation of the appropriate superposition integrals and the related space-
time Green's function. Plots of the time history of the radiated far-fields
are presented for various configurations and observation angles for
constant amplitude distributions on each array element.

CONTENTS

2

FIGURES

3

4

SECTION I

INTRODUCTION

The general approach to the simulation of a nuclear electromagnetic pulse using a radiating system consisting of planar sources has recently been considered from a qualitative point of view,[1] and methods of launching the required transient fields are currently under investigation. Such planar arrays consist of aperture sources having tangential electric fields which are excited in the appropriate time sequence and spacial distribution to obtain a desired far-field distribution. Techniques for launching the required waves for the simulation of an electromagnetic pulse have been discussed in previous work on pulser arrays.[2,3,4,5,6]

The purpose of this investigation is to analyze the transient radiated fields of planar arrays of sources which might be used to simulate a nuclear electromagnetic pulse (EMP). This work will not consider the problem associated with the excitation of the planar sources, and, consequently, the arrays studied will consist of sources with known aperture field distribution and "time-delay" distribution.

The first phase of the investigation consists of the analysis of the time-history of the far-fields of an array on N infinitely long slots in a perfectly conducting infinite plane as shown in Figure 1. The analysis of this array having known electric field distributions is based on a Green's function approach to the problem. A two-dimensional space-time Green's function for a single line of unit amplitude located on the plane is presented, and the actual time and amplitude distribution for each source is incorporated in the solution for the far-fields through the use of appropriate superposition integrals and the Green's function. The related in-

6
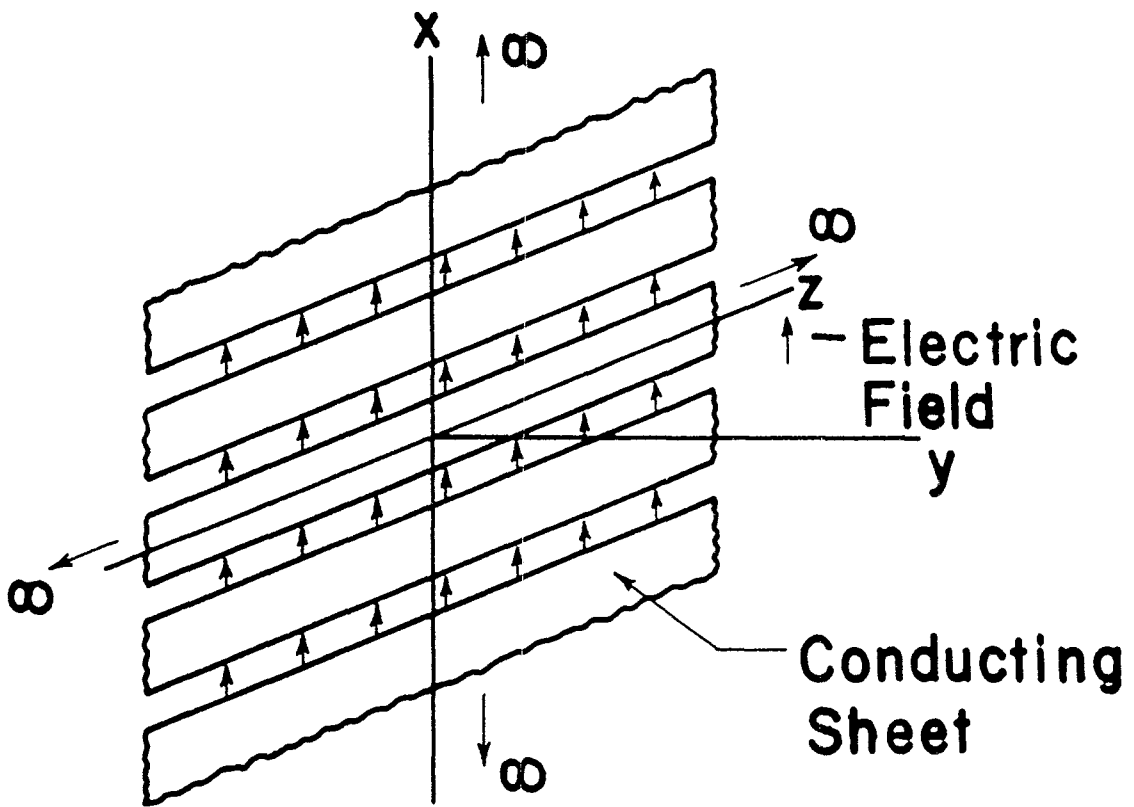
Figure 1. Planar array of two-dimensional slot sources.

vestigation of Sections II and III is based on the numerical evaluation
of this mathematical formulation.

SECTION II

TRANSIENT RADIATED FIELDS FOR A SINGLE SLOT
IN AN INFINITE PLANE

In this section, the transient radiated fields of a single slot are derived as a first step in the analysis of the array of planar slots in an infinite, perfectly conducting, ground plane as shown in Figure 1. Thus, the idealized problem consists of a known tangential electric field distribution in the plane where $y = 0$ which is outlined in Figure 2. For simplicity, only the electric field component, $E_x(x,t)$, is assumed over the slot width d, and the tangential electric field is assumed to be zero elsewhere on the plane as a result of the idealized conducting planes; however, the analysis of the related z component or the combinations of x and z components can be obtained in a similar manner. The two-dimensional coordinate system used in the mathematical formulation is shown in Figure 3 where the required distance factors are defined for the assumed source and field points. The medium is assumed to be that of free space, i.e. $\varepsilon = \varepsilon_0$, $\mu = \mu_0$, $\sigma = 0$ for $y > 0$.

Because the tangential field distribution is known everywhere on the $y = 0$ plane, the analysis reduces to a problem of developing mathematical expressions for the direct computation of the transient radiated fields. One approach to this problem is to invoke the surface-equivalence theorem to obtain equivalent surface currents from which the desired fields can be computed.[7] In this case, from Figures 2 and 3, only a magnetic surface current density exists, which is

$$\overline{M}_s = E_x(\overline{e}_x \times \overline{e}_y) \tag{1}$$

$$= E_x \overline{e}_z$$
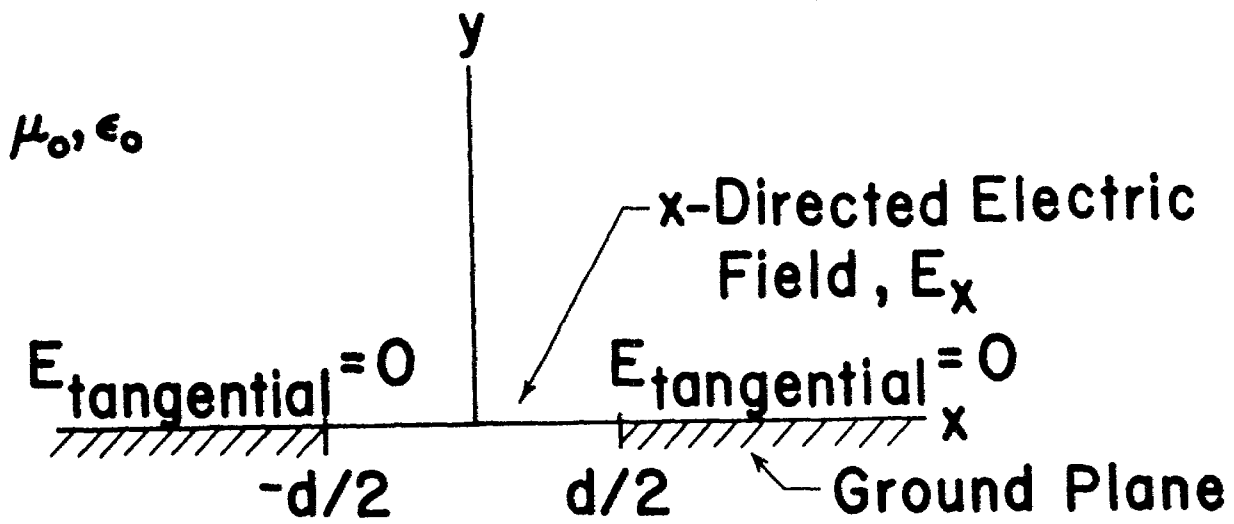
Figure 2. Geometry for slot in an infinite, perfectly conducting ground plane.

$$z,z'$$

$$(x',0,z')$$ $$|r-r'|$$

$$(x,y,z)$$

$$r'$$

$$r$$

$$y,y'$$

$$x,x'$$

$$r=(x^2+y^2+z^2)^{1/2}$$
$$r'=(x'^2+z')^2$$
$$|r-r'|-((x-x')^2+y^2+(z-z')^2)^{1/2}$$

Three-dimensional coordinates

$$\rho=(x^2+y^2)^{1/2}$$
$$R=((x-x')^2+y^2)^{1/2}$$
$$=((\rho\cos\phi-x')^2$$
$$+\rho^2\sin^2\phi)^{1/2}$$
$$\phi=\tan^{-1}(y/x)$$

$$y,y'$$

$$,(x,y)$$

$$\rho$$

$$R$$

$$\phi$$ $$(x',0)$$

$$x,x'$$

$$^-d/2$$ $$d/2$$
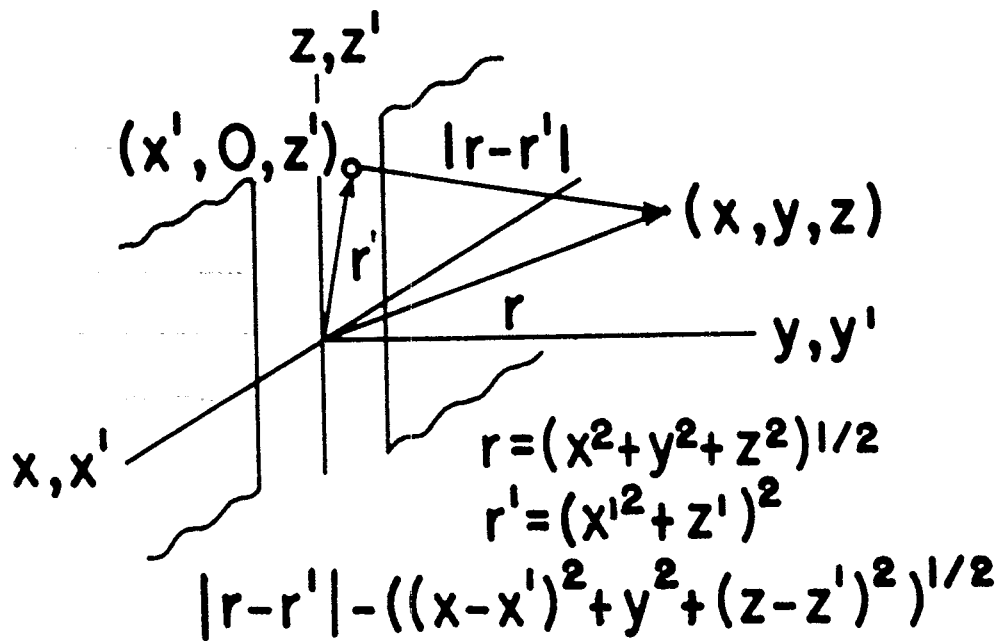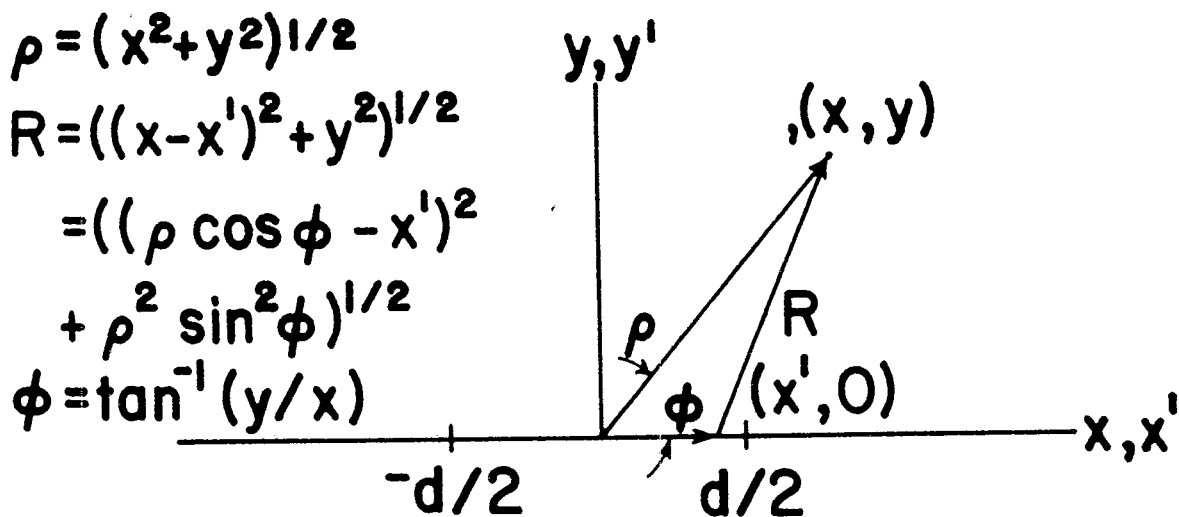
Two-dimensional coordinates

Figure 3. Coordinate Systems.

where E_x is the assumed electric field distribution existing on the infinite-length slot of the original problem and the $\bar{e}$'s are the unit vectors in the space. The equivalent problem for $y > 0$ consists of an electric conductor in the plane $y = 0$ (i.e., zero fields for $y < 0$) with a magnetic current density, $\bar{M}_s$, residing on the surface as depicted in Figure 4A. This equivalent problem can be formulated in terms of image theory to obtain a solution for the original boundary value problem where the total magnetic current density is

$$\bar{M} = \bar{M}_s \ \delta(y) = M_z \ \delta(y)\bar{e}_z = 2E_x\bar{e}_z \tag{2}$$

Hence, the equivalent problem of a sheet or ribbon of magnetic current as shown in Figure 4B can be used to analyze this two-dimensional problem.

An expression for the transient fields of the strip of magnetic current can be derived in terms of electric vector potential from Maxwell's equations for time dependent fields. Thus, since the problem involves only a source of magnetic current density, i.e., $\bar{J} = 0$, $\rho = 0$, $\rho_m = 0$, Maxwell's equations for this problem in free space become

$$\nabla \times \bar{H} = \varepsilon_0 \frac{\partial \bar{E}}{\partial t} \tag{3}$$

$$\nabla \times \bar{E} = -\mu_0 \frac{\partial \bar{H}}{\partial t} - \bar{M} \tag{4}$$

$$\nabla \cdot \bar{H} = 0 \tag{5}$$

and
$$\nabla \cdot \bar{E} = 0 \tag{6}$$

where all field quantities are functions of both time and space. In this homogeneous media, the electric field can be represented in terms of an electric vector potential, $\bar{F}$, as

12
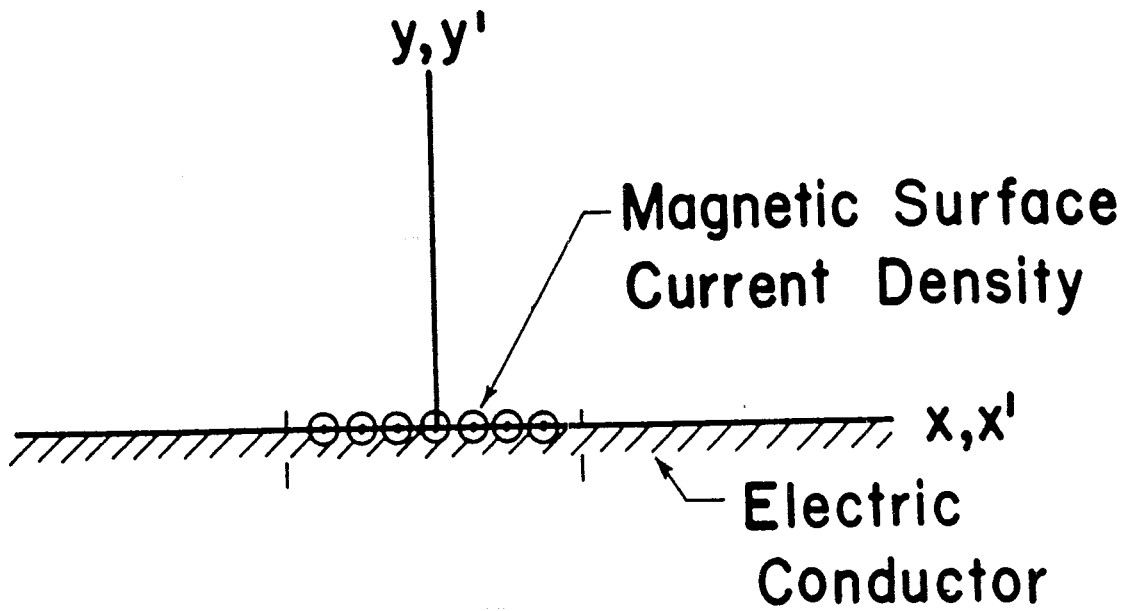
Figure 4A. Equivalent slot problem (z is pointing out
of the page).
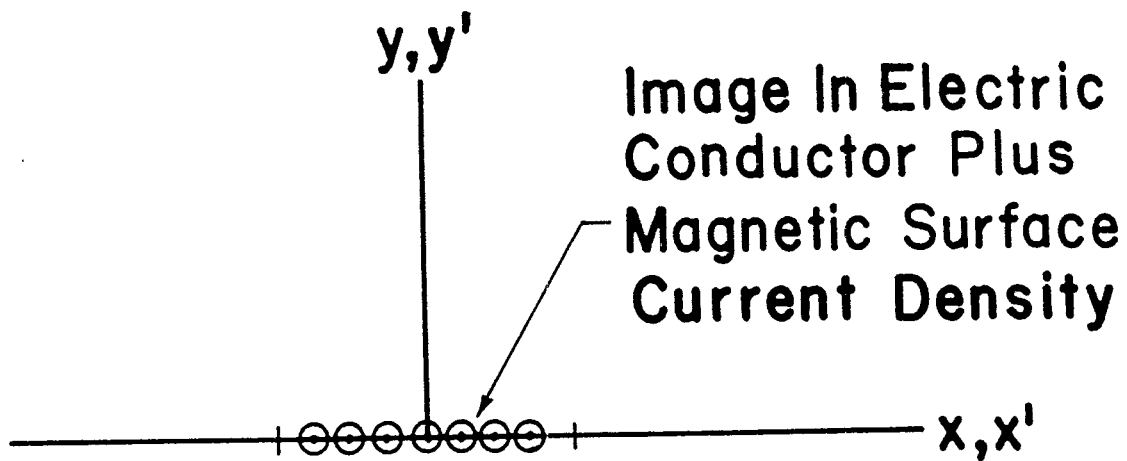
Figure 4B. Equivalent slot problem using image theory
(z is pointing out of the page).

$$\bar{E} = -\nabla \times \bar{F} \qquad (7)$$

because any divergenceless vector is the curl of some other vector. With this vector potential representation, the magnetic field can be represented in terms of $\bar{F}$ and the gradient of a scalar as

$$\frac{1}{\epsilon_0} \bar{H} = -\frac{\partial \bar{F}}{\partial t} - \nabla \phi_m \qquad (8)$$

where ϕ_m is the magnetic scalar potential. From the previous equations, it can be shown that the vector potential must satisfy the wave equation

$$c^2 \nabla^2 \bar{F} - \frac{\partial^2 \bar{F}}{\partial t^2} = -c^2 \bar{M}_s \delta(y) \qquad (9)$$

where a Lorentz gauge

$$\nabla \cdot \bar{F} + \frac{1}{c^2} \frac{\partial \phi_m}{\partial t} = 0 \qquad (10)$$

is assumed for $c = 1/(\mu_0 \epsilon_0)^{1/2}$ and $\bar{M} = \bar{M}_s(x,z,t)\delta(y)$.

The far fields can be computed in terms of the electric vector potential from the previous equations if equation (9) can be solved in terms of the known magnetic current density. In this case, it is desirable to reduce the potential wave equation with associated boundary conditions to an integral expression which is more amenable to numerical analysis. Such an integral expression can be obtained through the application of the Green's function method for the solution of differential equation.

The problem as shown in Figure 4 reduces to a two-dimensional problem in free space where the solution is valid for $y > 0$, and equation (9) becomes a scalar wave equation,

14

$$c^2 \nabla^2_{xy} f_z - \frac{\partial^2 f_z}{\partial t^2} = -c^2 M_z(x,z,t) \cdot \delta(y) \tag{11}$$

because from equation (2) only a z component of $\overline{M}_s$ exists. Since this is a free space problem, the related space-time Green's function is the principal solution of the general equation,

$$\nabla^2_{x'y'} G_0 - \frac{1}{c^2} \frac{\partial^2 G_0}{\partial \tau^2} = -\delta(x'-x, \; y'-y, \; \tau-t) \tag{12}$$

which has the solution[8]

$$G_0(x,y,t|x',y',\tau) = \begin{cases} 0, & R > c(t-\tau) \\[3mm] \dfrac{c}{2\pi} \left[\dfrac{1}{[c^2(t-\tau)^2 - R^2]^{1/2}} \right], & R < c(t-\tau) \end{cases} \tag{13}$$

for

$$R = \left[(x'-x)^2 + (y'-y)^2 \right] \tag{14}$$

as defined for a general unit line-source in both space and time in Figure 5A. Special boundary conditions at infinity and causality requirements dictate this solution where the variables of (11) have been interchanged to insure proper function dependence in the integral solution of equation (11). This Green's function is the characteristic two-dimensional solution for the scalar wave equation caused by an infinite line source excited at $\tau = t$. Actually, since the line consists of many point sources which radiate spherically, a response at some distance R_0 is first experienced at $\tau = t$ and subsequent response occurs for τ's $> t$; thus, the response decays according to equation (13) as shown in Figure 5B.

15
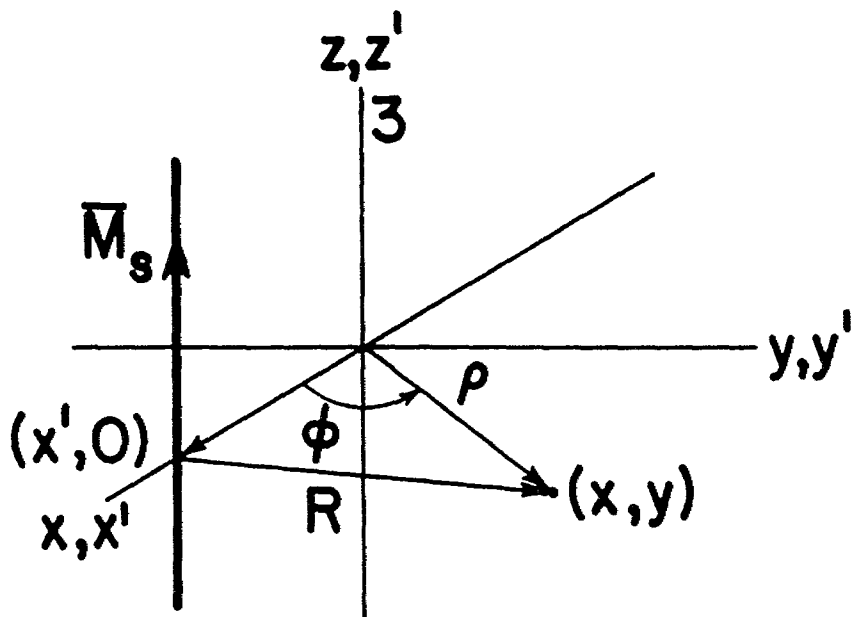
Figure 5A. Line source representation for a two-dimensional Green's function (pictured for y'=0).
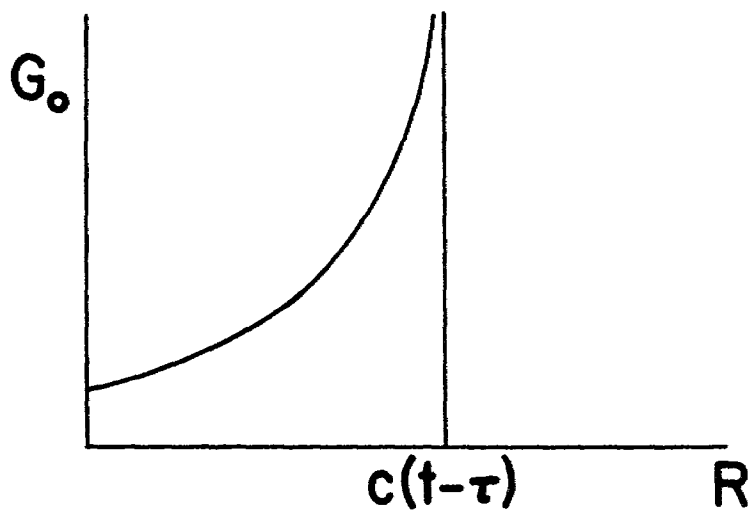
Figure 5B. Space-time Green's function for two-dimensional wave equation in free space.

Through the use of the appropriate Green's theorem and initial conditions, a solution of the inhomogeneous wave equation (11) can be expressed in terms of a superposition integral and this Green's Function as

$$f_z(x,y,t) = \int_0^T \int_{-\infty}^{\infty} \int_{-\infty}^{\infty} M_z(x',y',\tau) G_0(x,y,t|x',y',\tau) dx'dy'd\tau \qquad (15)$$

where the required free space boundary conditions and causality eliminate all contour contributions and T exceeds any time t at which the solution may be sought. Now, since the source exists only in the x-z plane (y=0), i.e. $M_z(x,y,\tau) = M_z(x,\tau) \delta(y)$, then equation (15) becomes

$$f_z(x,y,t) = \int_0^T \int_{-\infty}^{-\infty} M_z(x',\tau) G_0(x,y,t|x',0,\tau) dx,d\tau \qquad (16)$$

which is an integral formula for computing the electric vector potential for planar two-dimensional sources of known electric field distribution through the use of equation (2).

The time dependent or transient fields radiated in the far-field of the two-dimensional, planar source can be expressed in terms of equation (16) with the aid of the expressions of equations (7) and (8). Thus,

$$E = -\nabla \times \bar{e}_z \int_0^T \int_{-\infty}^{\infty} M_z(x',\tau) G_0(x,y,t|x',0,\tau) dx'd\tau \qquad (17)$$

and

$$H = -\varepsilon_0 \frac{\partial}{\partial t} \left[\bar{e}_z \int_0^T \int_{-\infty}^{\infty} M_z(x',\tau) G_0(x,y,t|x',0,\tau) dx'd\tau \right] \qquad (18)$$

where the scalar potential component of the $\bar{H}$-field equation is zero in this two-dimensional problem. In the three-dimensional case, this term can be dropped because it has a higher inverse power of distance than the time derivative term, and, therefore, the scalar potential contribution is smaller than the vector potential contribution to the field at large distances. However, the scalar potential contribution could be expressed in terms of the vector potential using the Lorentz condition of equation (10) and, thereby, included in a complete three-dimensional formulation.

The field formulations of equations (17) and (18) are not readily solved using numerical techniques in their existing forms, but for some simple magnetic current density representations these expressions can be reduced to forms with tractable numerical solutions. One simplification which greatly reduces the numerical computation required is the use of a step-function dependence in time such that

$$M_z(x,\tau) = M_z(x)\, u(\tau) \tag{19}$$

where other time dependences can be obtained from a superposition integral based on the summation of step function responses.[9] For this case of a planar array excited at $\tau = 0$ with a step function dependence, the field expression becomes

$$\bar{E} = -\nabla \times \bar{e}_z \int_{-\infty}^{\infty} M_z(x') \left[\int_0^T G_0\, d\tau \right] dx' \tag{20}$$

and

$$\bar{H} = -\varepsilon_0 \frac{\partial}{\partial t} \left[\bar{e}_z \int_{-\infty}^{\infty} M_z(x') \left[\int_0^T G_0\, d\tau \right] dx' \right] \tag{21}$$

18

where the functional dependence of the Green's function has been dropped for simplicity. In the present form, equations (20) and (21) require double integration to compute the field quantities which is usually undesirable in numerical analysis; however, the integral in the dummy time variable of the Green's function can be obtained in a closed form. From equations (20) and (13), this integral becomes

$$G_1 = \frac{c}{2\pi} \int_0^{t-R/c} \frac{1}{[c^2(t-\tau)^2-R^2]^{1/2}}$$

(22)

and, if the change of variables $\eta = t-\tau$, $d\eta = -d\tau$, and $R/c = b$ are used, then

$$G_1 = \frac{1}{2\pi} \int_t^b \frac{-d\eta}{(\eta^2-b^2)^{1/2}}$$

(23)

Note that the upper limit of (23) is evaluated at $T = t-R/c$ because $G_0=0$ for $T > t-R/c$. The unit step response, G_1, of an infinitely long line of magnetic charge density can be obtained in a closed form using the indefinite integral form,[10]

$$\int dx/(x^2-a^2)^{1/2} = \ell n(x+(x^2-a^2)^{1/2})$$

as

$$G_1(x,y,t|x') = \frac{1}{2\pi} \ell n \left[\frac{t + \sqrt{t^2-(R/c)^2}}{R/c} \right]; \quad t > R/c$$

(24)

Finally, the field expressions of equations (20) and (21) can be written in terms of the step response of the infinitely long line (equation 23) as

$$E = -\nabla \times \overline{e}_z \int_{-\infty}^{\infty} M_z(x') \, G_1(x,y,t|x')dx'$$

(25)

and

$$\bar{H} = -\varepsilon_0 \frac{\partial}{\partial t}\left[\bar{e}_z \int_{-\infty}^{\infty} M_z(x') \, G_1(x,y,t|x')dx'\right] \tag{26}$$

The individual field components can now be obtained in cylindrical coordinates defined in Figure 3 as

$$E_\phi = \int_{-\infty}^{\infty} M_z(x') \, \frac{\partial G_1}{\partial \rho} \, dx' \tag{27}$$

$$E_\rho = -\int_{-\infty}^{\infty} M_z(x')\frac{\partial G_1}{\rho \partial \phi} \, dx' \tag{28}$$

and

$$H_z = -\varepsilon_0 \int_{-\infty}^{\infty} M_z(x') \, \frac{\partial G_1}{\partial t} \, dx' \tag{29}$$

where differentiation under the integral sign is valid in all cases because the limits and variable of integration are independent of the differentiation variables. If the chain rule for differentiation of composite functions is used, the partial derivatives of the integrands of equations (27) and (28) can be evaluated as

$$K_1(x,y,t,x') = \frac{\partial G_1}{\partial \rho} = \frac{\partial G_1}{\partial R} \cdot \frac{\partial R}{\partial \rho}$$

$$- \frac{[t(t^2-(R/c)^2)^{1/2}+t^2][\rho-x'\cos\phi]}{2\pi \, R^2[t(t^2-(R/c^2)^{1/2}+t^2 - (R/c)^2]} \tag{30}$$

and $\quad K_2(x,y,t,x') = \frac{\partial G_1}{\rho \partial \phi} = \frac{\partial G_1}{\rho \partial R} \cdot \frac{\partial R}{\partial \phi}$

$$= \frac{-[t(t^2-(R/c)^2)^{1/2}+t^2]x'\sin\phi}{2\pi R^2[t(t^2-(R/c)^2)^{1/2}+t^2-(R/c)^2]} \tag{31}$$

where G_1 and R are differentiable over the region $t > R/c$ and R and ρ are defined in the polar coordinates of Figure 3 as

$$R = [\rho^2 \sin^2\phi + (\rho \cos\phi - x')^2]^{1/2} \tag{32}$$

and

$$\rho = [x^2 + y^2]^{1/2} \tag{33}$$

such that

$$\frac{\partial R}{\partial \rho} = \frac{\rho - x' \cos\phi}{R} \tag{34}$$

and

$$\frac{\partial R}{\partial \phi} = \frac{\rho x' \sin\phi}{R} \tag{35}$$

Equations (27), (28), and (29) can now be expressed in simplified terms as

$$E_\phi = \int_{-\infty}^{\infty} M_z(x') \, K_1(x,y,t,x') dx' \tag{36}$$

$$E_\rho = -\int_{-\infty}^{\infty} M_z(x') \, K_2(x,y,t,x') dx' \tag{37}$$

and

$$H_z = -\int_{-\infty}^{\infty} M_z(x') \, K_3(x,y,t,x') dx' \tag{38}$$

where K_1 and K_2 are defined in equations (30) and (31) and

$$K_3(x,y,t,x') = \partial G_1/\partial t \cdot \varepsilon_0$$

$$= \frac{\varepsilon_0}{2\pi} \frac{1}{(t^2 - (R/c)^2)^{1/2}} \tag{39}$$

Equations (36), (37), and (38) are general expressions for the three far-field components produced by a two-dimensional source of z-directed magnetic current density for an assumed step function excitation in time.

These field components can be related to known x-directed electric field distributions through the use of equation (2).

SECTION III

SINGLE- AND MULTIPLE- ELEMENT ARRAYS OF SLOTS
WITH CONSTANT SOURCE DISTRIBUTION

SINGLE SLOTS

In this investigation, slot sources of known constant electric

field distribution are of primary interest. Consequently, as a first

step in the solution of the related problem, the single slot with an

x-directed electric field distribution such that

$$M_z(x') = 2E_0[u(x'+d/2) - u(x'-d/2)] \tag{40}$$

is analyzed. The transient field components for the single slot of

Figures 3 and 4B with constant source distribution are, from equations (36)

through (38) and (40),

$$e_\phi = \frac{E_\phi}{E_0} = 2 \int_{-d/2}^{d/2} K_1(x,y,t,x')dx' \tag{41}$$

$$e_\rho = \frac{E_\rho}{E_0} = -2 \int_{-d/2}^{d/2} K_2(x,y,t,x')dx' \tag{42}$$

and
$$h_z = \frac{Z_0 H_z}{E_0} = -2Z_0 \int_{-d/2}^{d/2} K_3(x,y,t,x')dx' \tag{43}$$

where each component has been normalized to an appropriate constant and Z_0

is the characteristic impedance of free space.

The expressions of equations (41), (42), and (43) are of the super-

position or convolution type integral form which can readily be represented

in graphical form, as shown in Figure 6. In this case, these problems

consist of the convolution of a constant amplitude pulse function in space

(x') and the appropriate sharply peaked, kernel function. Integrable

Kernel Function

$0 < \phi < \pi/2$

Normalized Field Distribution

d/2   O   ⁻d/2   ⁻x'
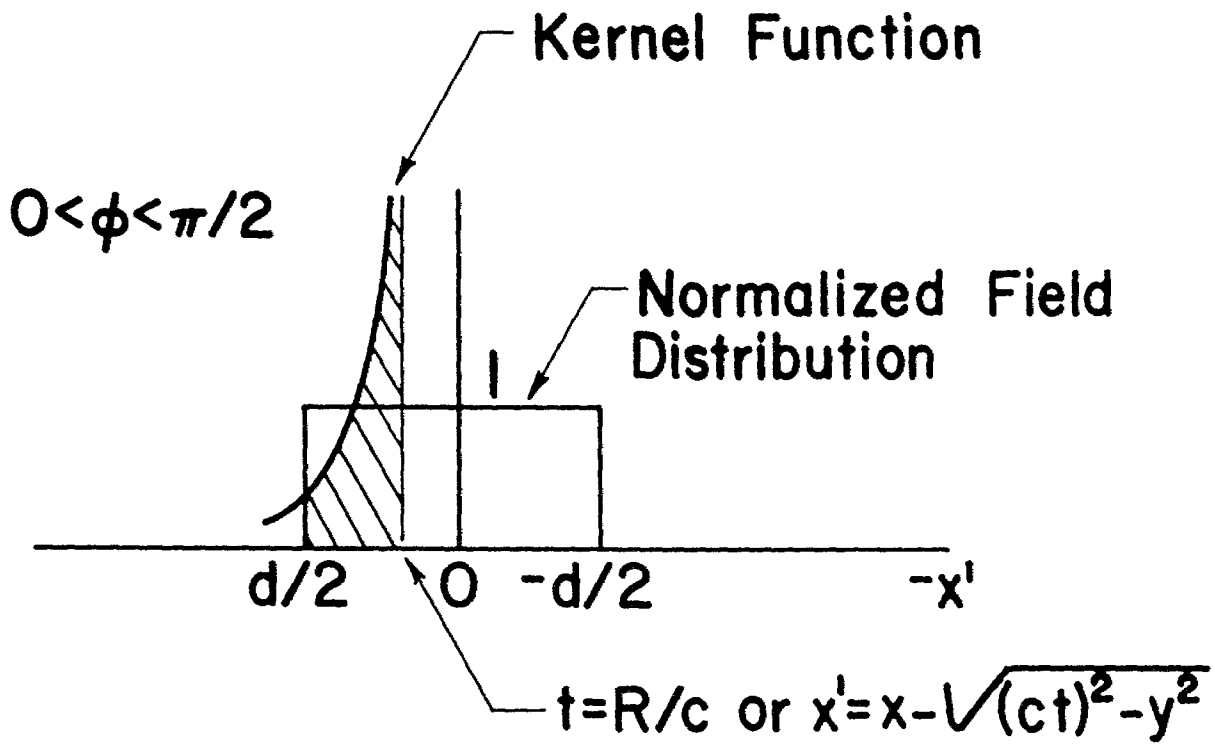
$t = R/c$ or $x' = x - \sqrt{(ct)^2 - y^2}$

Figure 6.   Graphical representation of the field integrals
for a single strip.

singularities of the kernel functions do appear in the spatial coordinate x' for t=R/c where R is the distance between the field point and source point. Thus, for a given point in space (x,y) and a time (t), the magnitude of the field is related to the total area underneath the curve defined by the shaded section in Figure 6. For the general case ($\phi > 0$), a solution which increases from zero to a maximum value followed by a monotonically decreasing magnitude as a function of time can be obtained for the e_ϕ and h_z field components. However, the expressions for the e_ρ component is a direct function of x' and sin ϕ (see equation 31), and this component vanishes on the plane $y = 0$ ($\phi = 0,\pi$). In addition, this functional dependence can change the polarity of the integrand of equation (42) because x' is an odd function which leads to field expressions for the e_ρ component that are either positive or negative depending on geometry of the problem. The magnitude of the time-history of the e_ρ component is similar to that of the e_ϕ and h_z field components unless the origin of the coordinate system lies within the slot. The single slot of Figure 4B is symmetrically spaced about the center of the coordinate system, and, as a result of the "oddness" of the integrand, the time-history of the e_ρ component has both positive and negative excursions.

The rise-time of each of the waveforms of these field components is related to the "delay-time" between field contributions propagating from the closest and furthest source points on the slot in relation to the field point (See Figure 3 for geometrical configuration). This rise-time*, t_r, can be defined as the time required for the field to increase from zero to one-hundred percent of its maximum or peak value. For narrow slots, it is a direct function of the width for e_ϕ, e_ρ (in all but the special cases),

---

*This rise-time definition is valid only for single slot element responses which increase monotonically as a function of time to some peak value.

and h_z as is anticipated from the "turn on" points in the graphical representation of spatial convolution in Figure 6. For large distances, it can be shown that the previously defined rise-time for these field components can be expressed in normalized form as

$$\tau_r = t_r/(R_0/c) = (d/R_0)\cos\phi \qquad (44)$$

where $R \simeq R_0 - d\cos\phi$, t_r is the total rise-time, R_0 is the distance from the center of the slot to the field point, and d is the total width of the slot. Equation (44), though approximate, clearly indicates that the normalized rise-time is a sensitive function of the angle ϕ, particularly around $\phi = \pi/2$, and that the smallest rise times are obtained for broadside propagation ($\phi = \pi/2$) and small width-to-distance ratios.

An approximate expression for late-time behavior of the e_ϕ component of the radiated electromagnetic at large distances can be obtained directly from the magnetic field, h_z. In the far-field, i.e. $d/R_0 \ll 1$, the electric field is related to the magnetic field by the characteristic impedance of free space; thus, from equations (39) and (43),

$$e_\phi \simeq -\frac{1}{\pi} \int_{-d/2}^{d/2} \frac{dx'}{[(ct)^2 - R^2]^{1/2}} \qquad (45)$$

when $t > R/c$ such that a response from each point on the slot is experienced at the field point. Equation (45) can now be expressed as

$$e_\phi = -\frac{1}{\pi} \int_{-d/2}^{d/2} \frac{dx'}{[a + bx' + cx'^2]^{1/2}} \qquad (46)$$

which is integrable in a closed form, where from the geometry of the single slot,

26

$$a = (ct)^2 - R_0^2$$

$$b = 2R_0 \cos\phi \qquad (47)$$

and
$$c = -1$$

This integral has a solution

$$\int \frac{dx'}{[a + bx' + cx'^2]^{1/2}} = \frac{1}{\sqrt{-c}} \sin^{-1} \frac{-2cx-b}{\sqrt{b^2-4ac}} \qquad (48)$$

thus, an approximate expression for the electric field component in the ϕ direction is obtained in the form

$$e_\phi = -\frac{1}{\pi} \left[\sin^{-1} \frac{\cos\phi+d/2R_0}{\sqrt{\cos^2\phi+\tau_0^2-1}} - \sin^{-1} \frac{\cos\phi-d/2R_0}{\sqrt{\cos^2\phi+\tau_0^2-1}} \right] \qquad (49)$$

where $\tau_0 = t/(R_0/c)$, and

$$\tau_0 \geq [1+(d/R_0)\cos\phi+(d/R_0)^2]^{1/2} \qquad (50)$$

for late-time behavior. Of course, equation (49) is related to an exact closed-form expression for h_z based on equation (45), i.e. $e_z = Z_0 h_z$; and for $\phi = \pi/2$, the equation (49) reduces to a form

$$e_\phi = -\frac{2}{\pi} \sin^{-1} \frac{d/2R_0}{\sqrt{\tau_0^2-1}} \qquad (51)$$

where it can easily be seen that these components decay in time. Note that for $\tau_0 = [1+(d/1R_0)^2]^{1/2}$ in equation (51), which is at the peak of the waveform,

$$e_\phi = -1 \qquad (52)$$

27

for the special case when $\phi \equiv \pi/2$. In addition, it is recognized that equation (49) is quite general and can be employed to compute the complete late-time behavior after the peak has occurred for both the h_z and e_ϕ components for small slot-width-to-distance ratios.

A numerical solution procedure for computing the time-history of the field components of equations (41), (42), and (43) has been developed and programmed for a digital computer. This procedure is a straightforward application of numerical integration using an open-ended Gauss quadrature formula for the treatment of the singularities of the kernel functions. The application of numerical integration in time-domain problems dis-cretizes the representation of the integral, i.e., the total field is the sum of weighted, time-shifted contributions from a finite set of points on the slot because of the inherent time-delay between integration points. As a result, care must be exercised to insure that the spatial variable of integration is "sampled" at a sufficient number of points to obtain a convergent integration, especially in the rise-time region. This problem is pronounced for small observation time increments, and an insufficient number of integration points results in an irregular waveform consisting of a serrated shape during the early-time response of the function.

The time-history of the computed field components using this numerical procedure is characterized in Figures 7 through 15 as a function of normalized parameters

$$\tau_0 = t/(R_0/c) \qquad (53)$$

and $\phi/(\pi/2)$ for three slot-width-to-distance ratios, d/R_0, along with approximate fields from equation (49). As can be seen, each e_ϕ and h_z
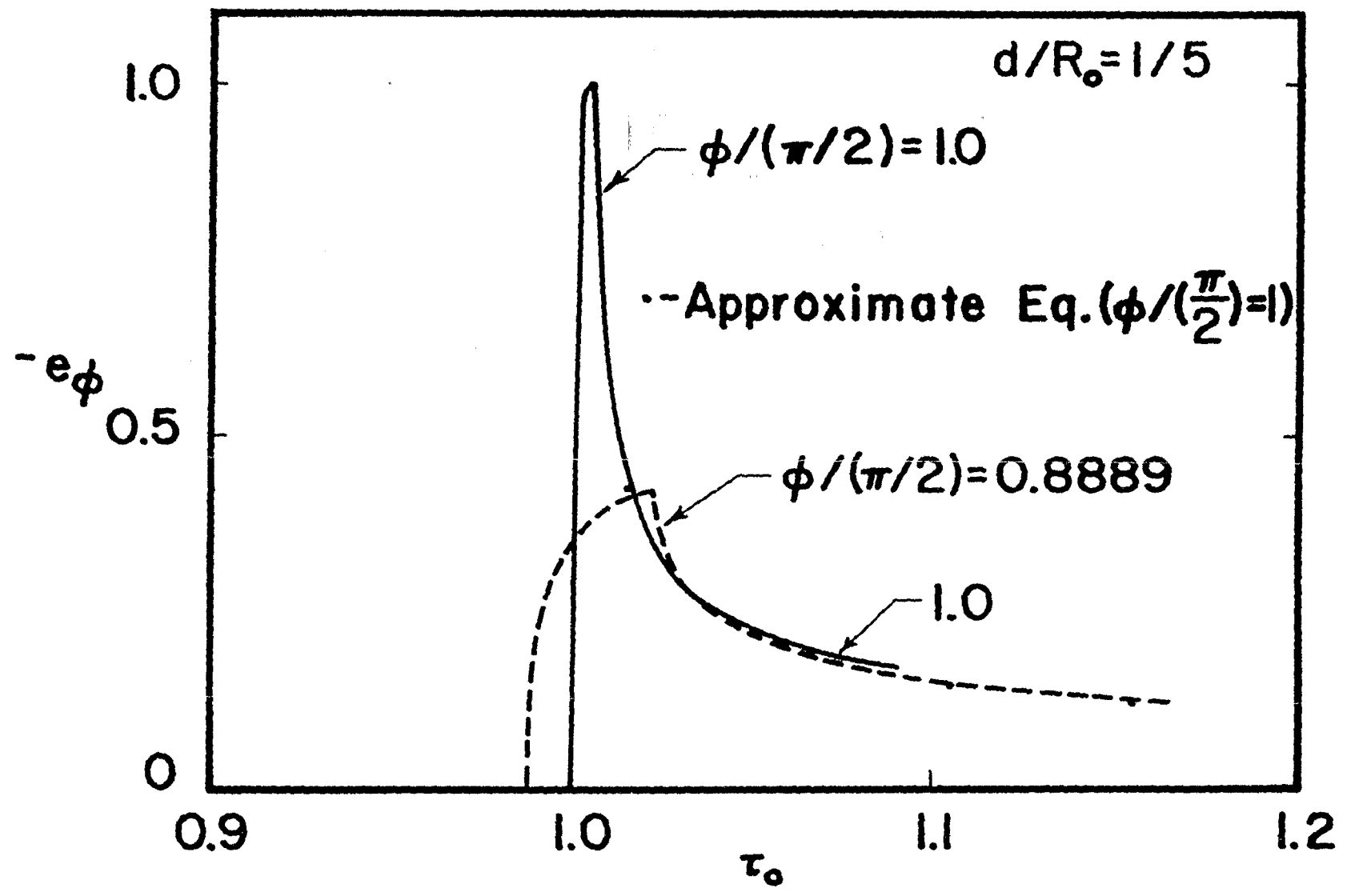
28

Figure 7A. e_ϕ vs. τ_0 for $d = 1/5$ with the parameter $\phi/(\pi/2) > 0.75$.
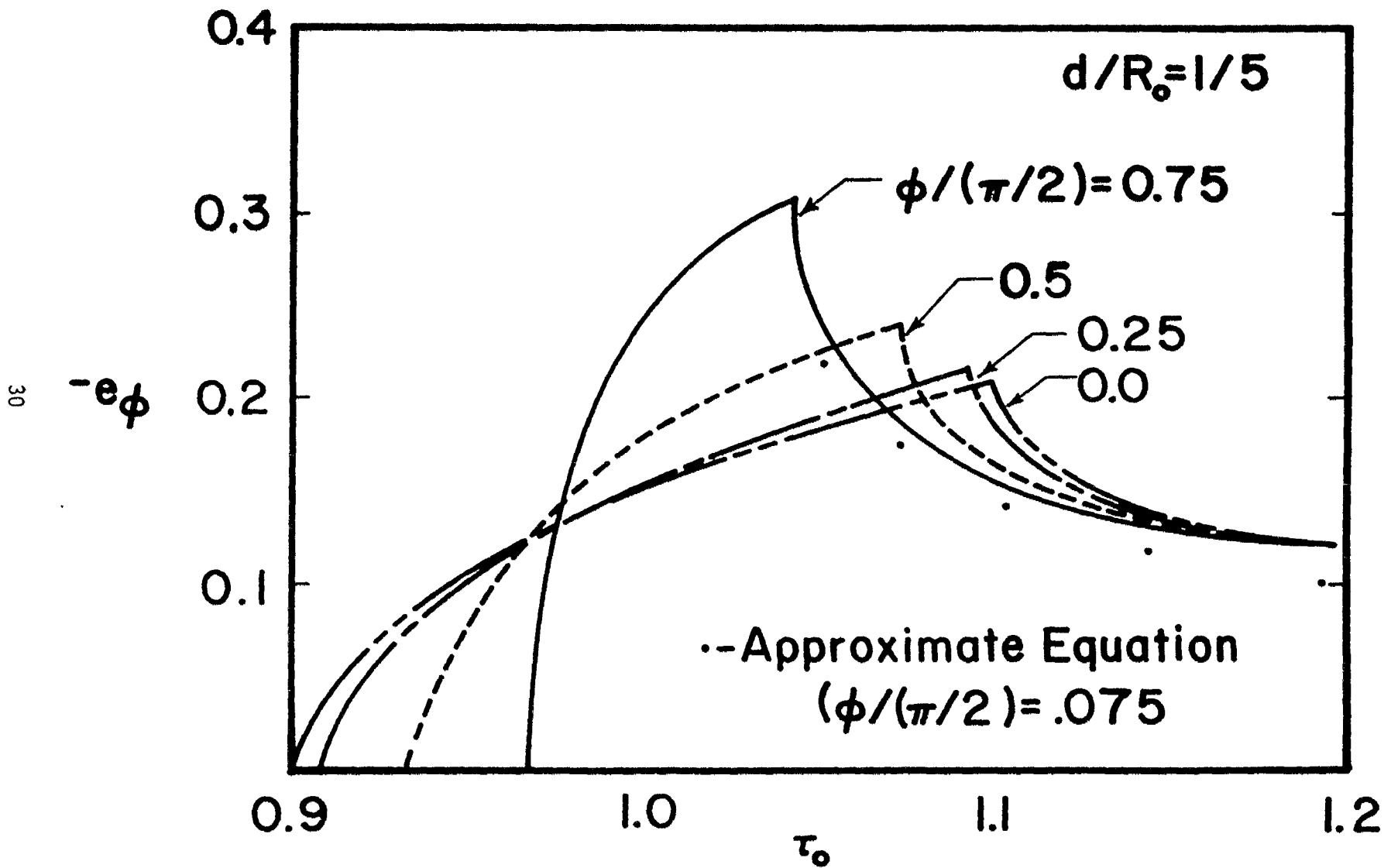
Figure 7B. e_ϕ vs. τ_0 for $d/R_0 = 1/5$ with the parameter $\phi/(\pi/2) \leq 0.75$.

Figure 8A. h_z vs. τ_0 for $d/R_0 = 1/5$ with the parameter $\phi/(\pi/2) > 0.75$.

Figure 8B. h_z vs. τ_0 for $d/R_0 = 1/5$ with the parameter $\phi/(\pi/2) \leq 0.75$.

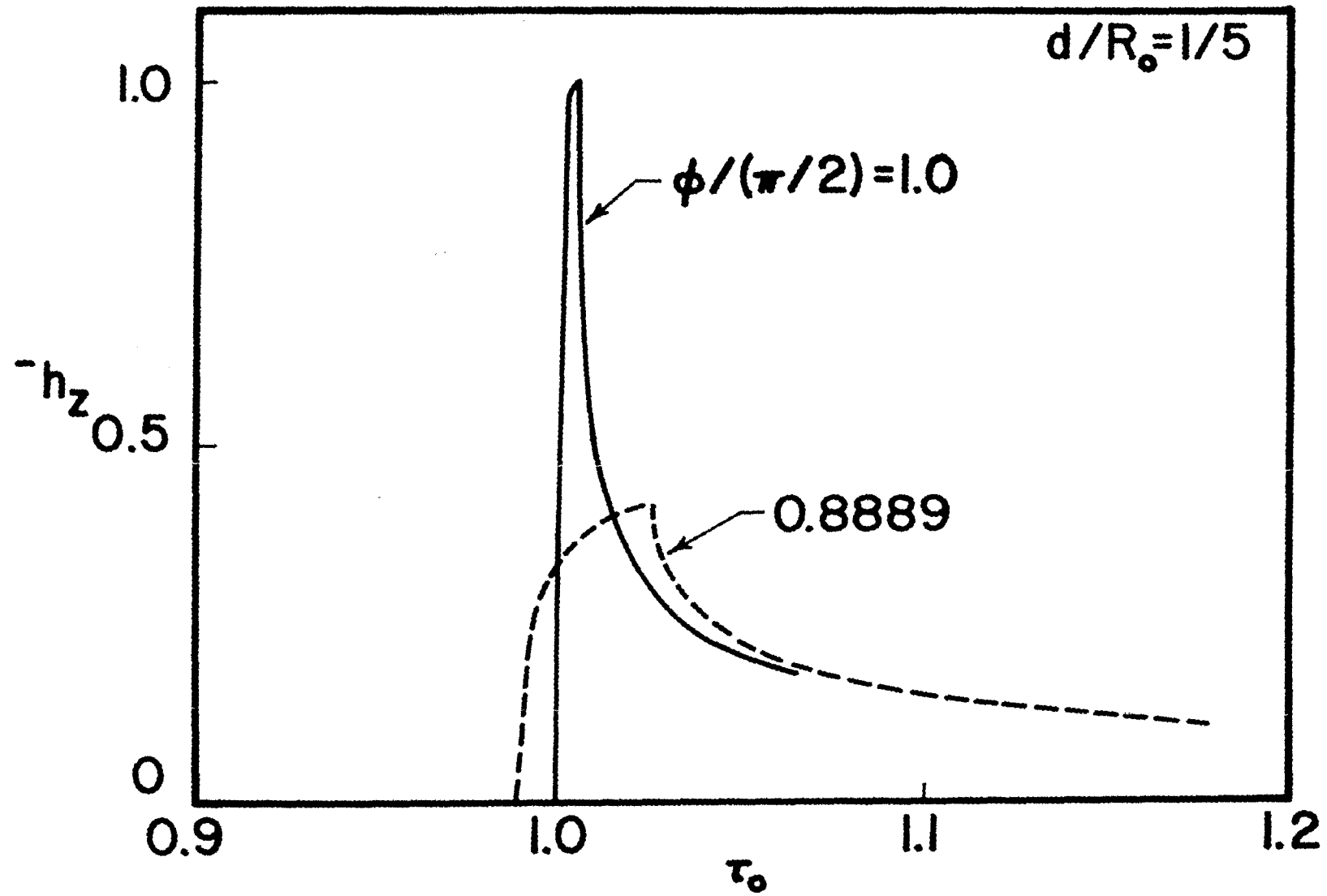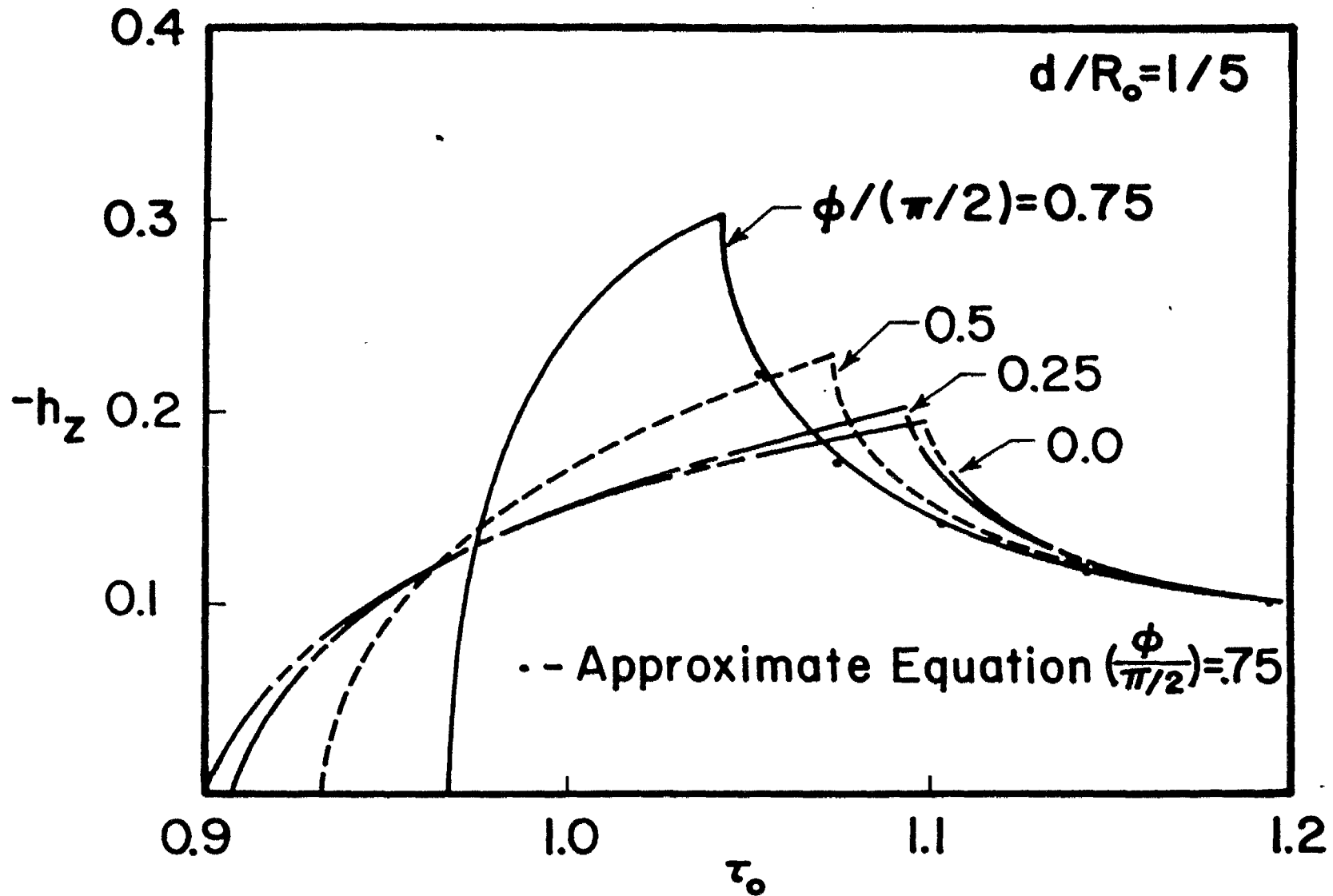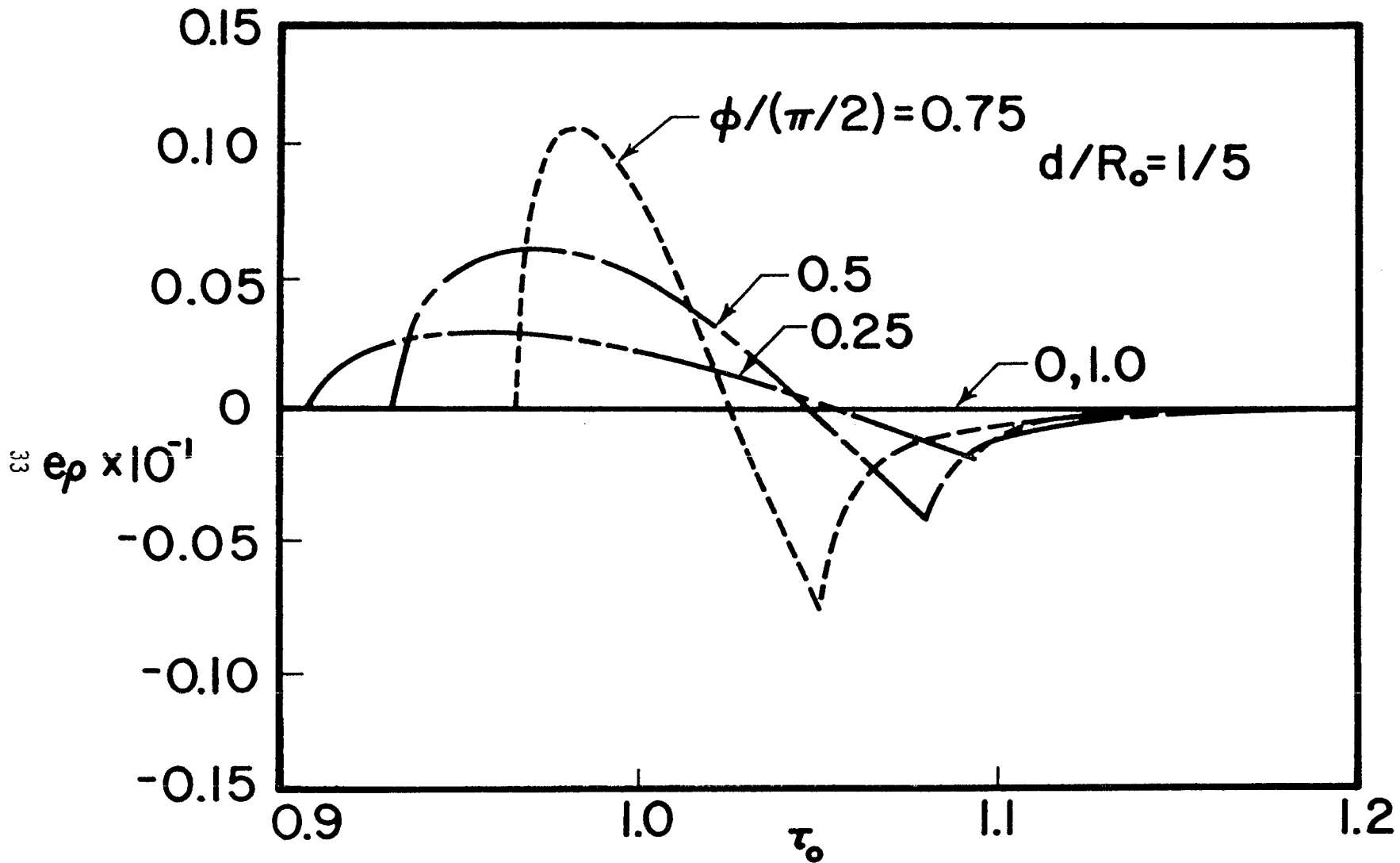Figure 9. e_ρ vs. τ_0 for $d/R_0 = 1/5$ with ϕ as a parameter.
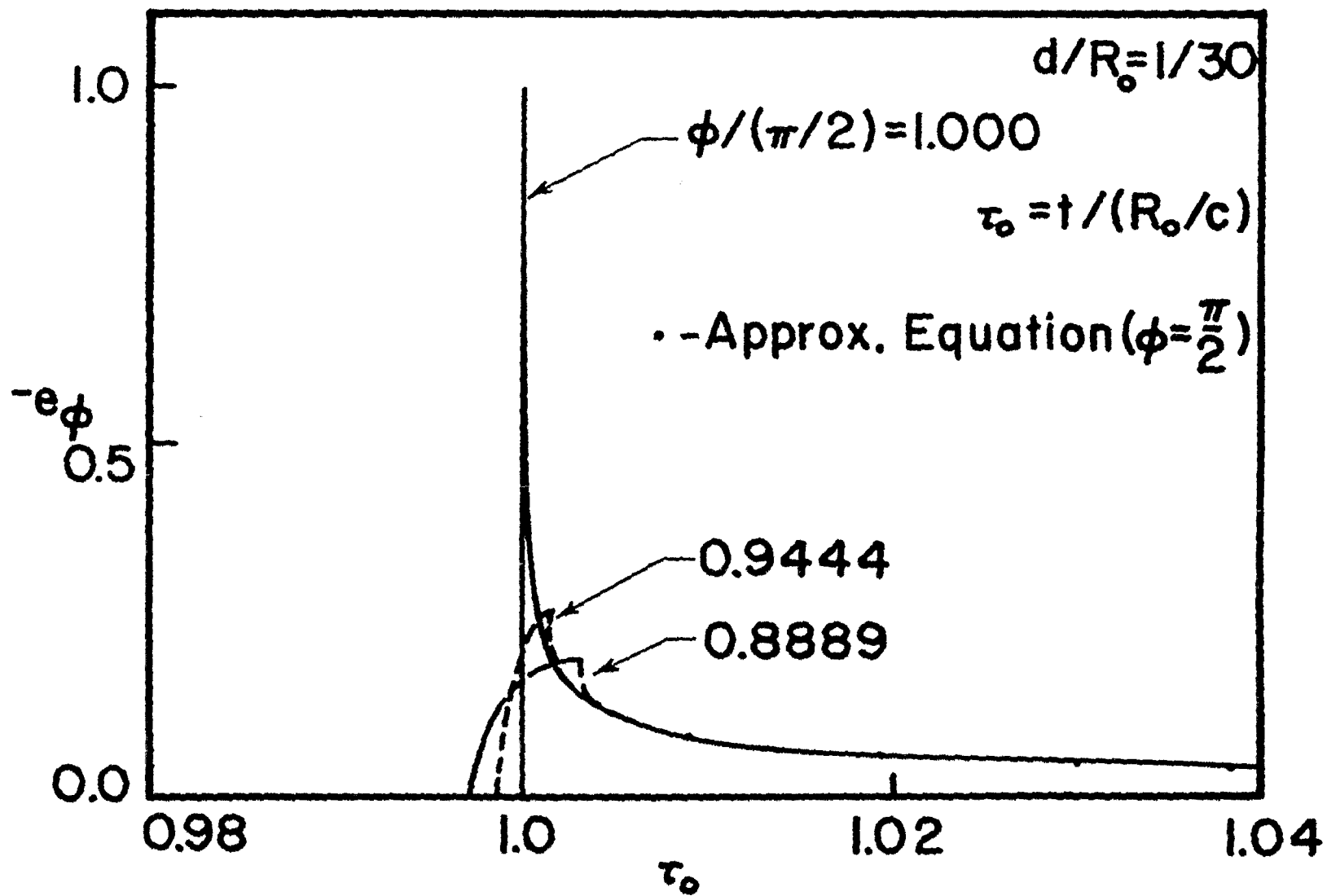
Figure 10A. e_ϕ vs. τ_0 for $d/R_0 = 1/30$ with the parameter $\phi/(\pi/2) \geq 0.75$.

The figure shows a plot with the following labels:

- $d/R_o = 1/30$
- $\phi/(\pi/2) = 1.000$
- $\tau_o = t/(R_o/c)$
- $\cdot$ - Approx. Equation $\left(\phi = \frac{\pi}{2}\right)$
- 0.9444
- 0.8889

Y-axis labeled $^-e_\phi$ with values 0.0, 0.5, 1.0

X-axis labeled τ_o with values 0.98, 1.0, 1.02, 1.04

Figure 10B. e_ϕ vs. τ_0 $d/R_0 = 1/30$ with the parameter $\phi/(\pi/2) \leq 0.75$.

Figure 11A. h_z vs. τ_0 for $d/R_0 = 1/30$ with the parameter $\phi/R_0 > 0.75$.

Figure 11B. h_z vs. τ_0 $d/R_0 = 1/30$ with the parameter $\phi/(\pi/2) \leq 0.75$.

The figure shows curves labeled $d/R_o = 1/30$, $\phi/(\pi/2) = 0.75$, 0.5, 0.25, 0.0. The vertical axis is $-h_z \times 10^{-1}$ with values 0.5, 1.0, 1.4. The horizontal axis is τ_0 with values 0.98, 1.0, 1.02, 1.04.
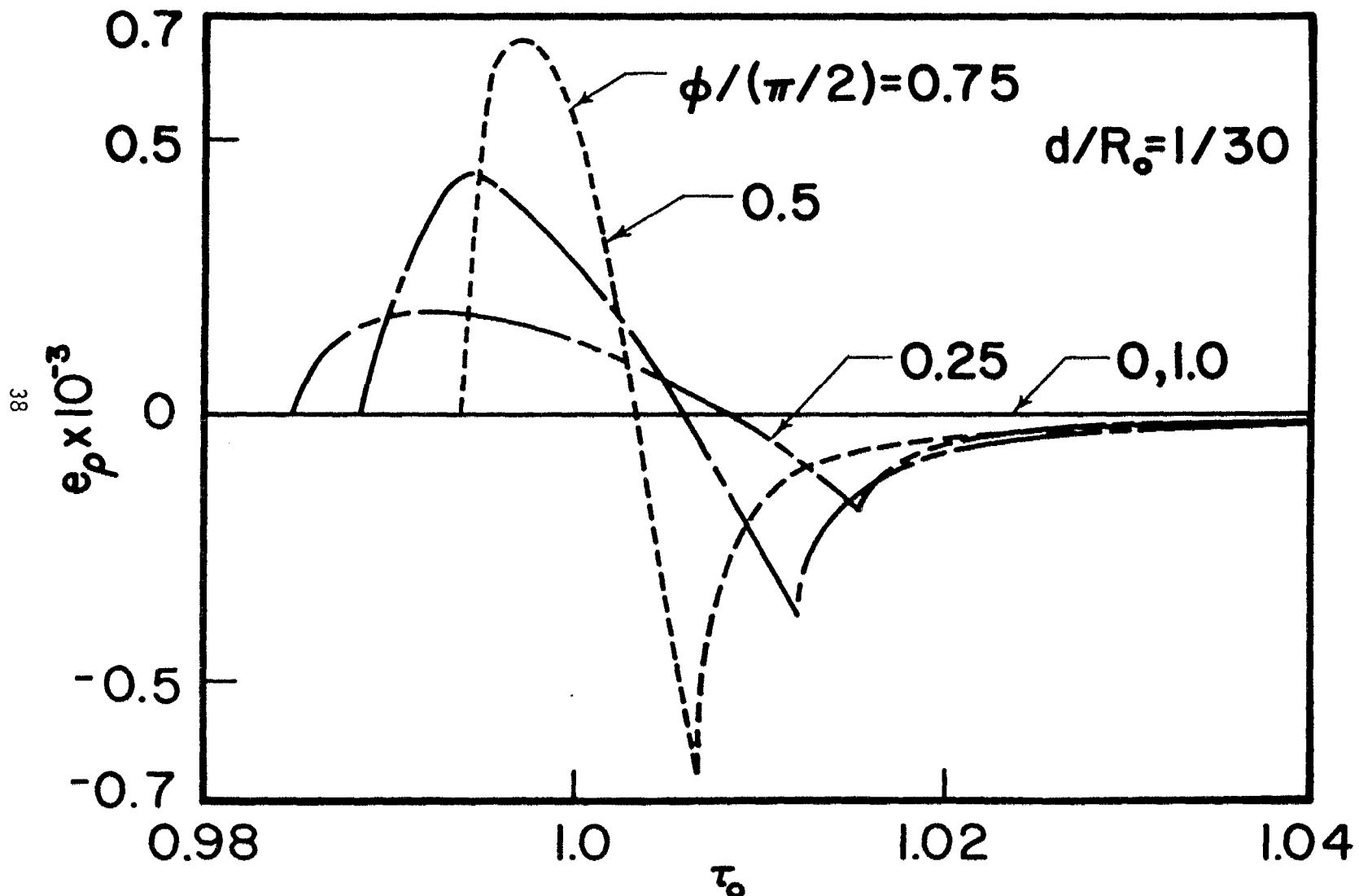
Figure 12. e_ρ vs. τ_0 for $d/R_0 = 1/30$ with ϕ as a parameter.

Figure 13A. e_ϕ vs. τ_0 for $d/R_0 = 1/300$ with the parameter $\phi/(\pi/2) > 0.75$.
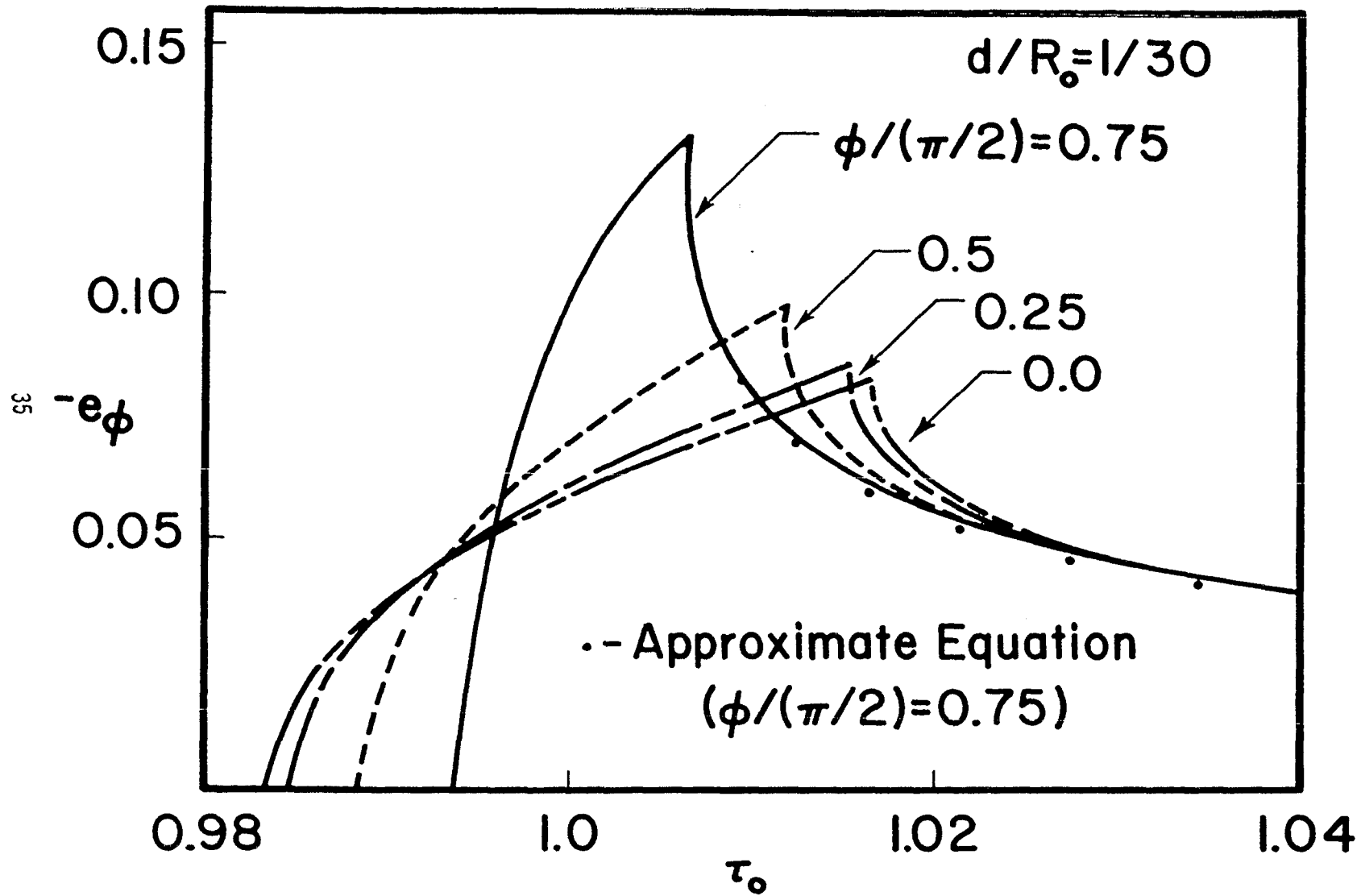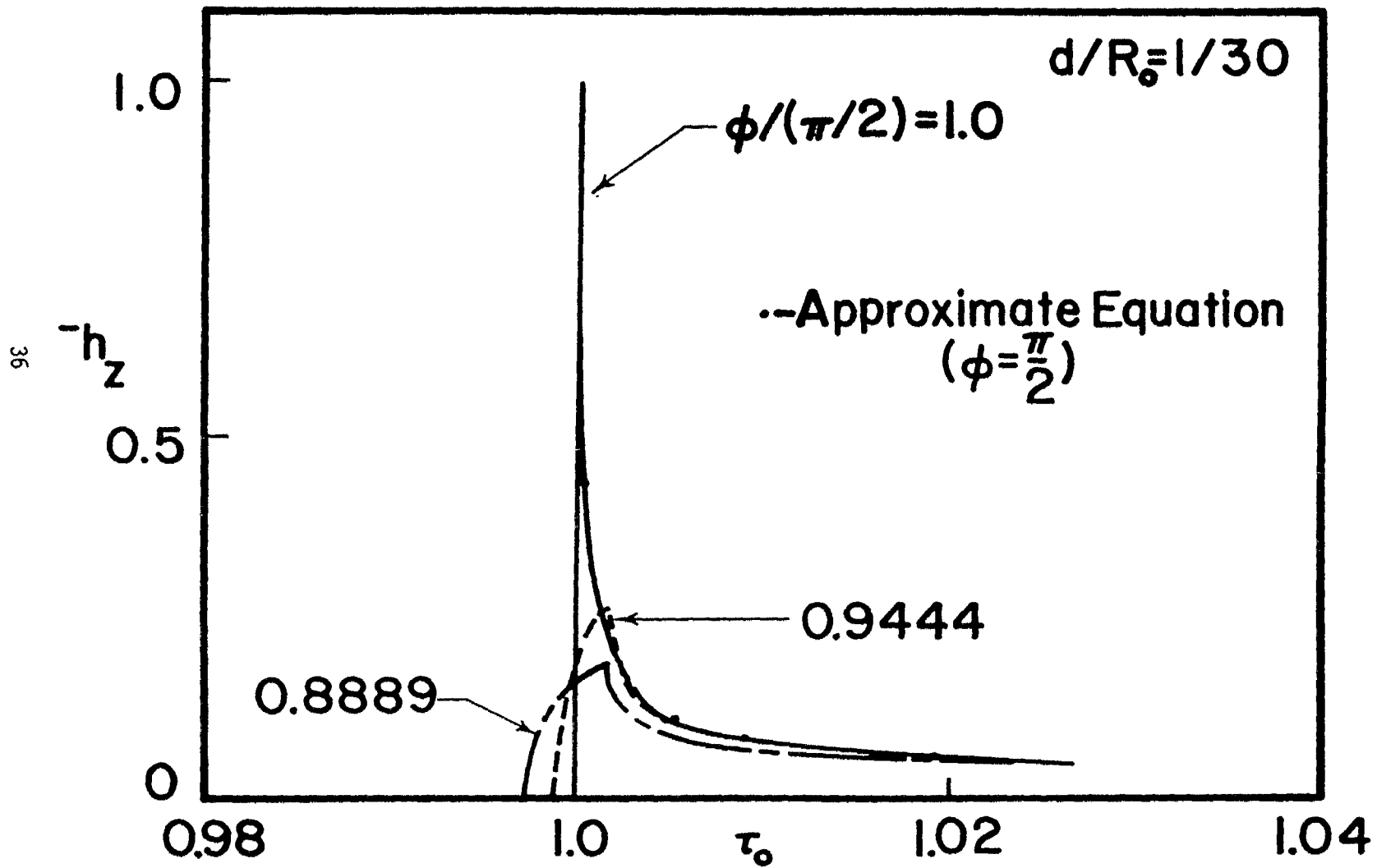
Figure 13B. e_ϕ vs. τ_0 for $d/R_0 = 1/300$ with the parameter $\phi/(\pi/2) \leq 0.75$.

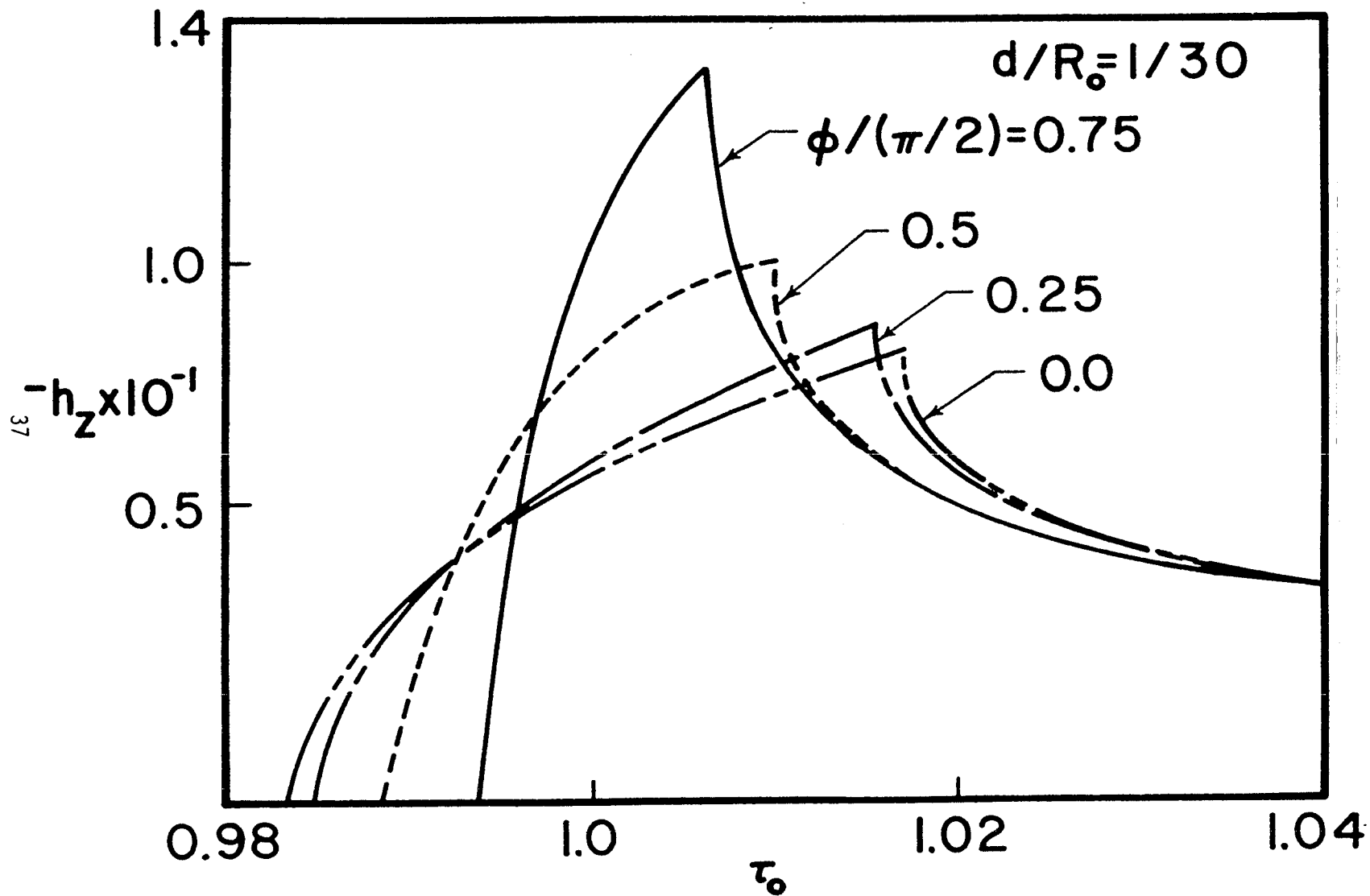Figure 14A. h_z vs. τ_0 for $d/R_0 = 1/300$ with the parameter $\phi/(\pi/2) > 0.75$.

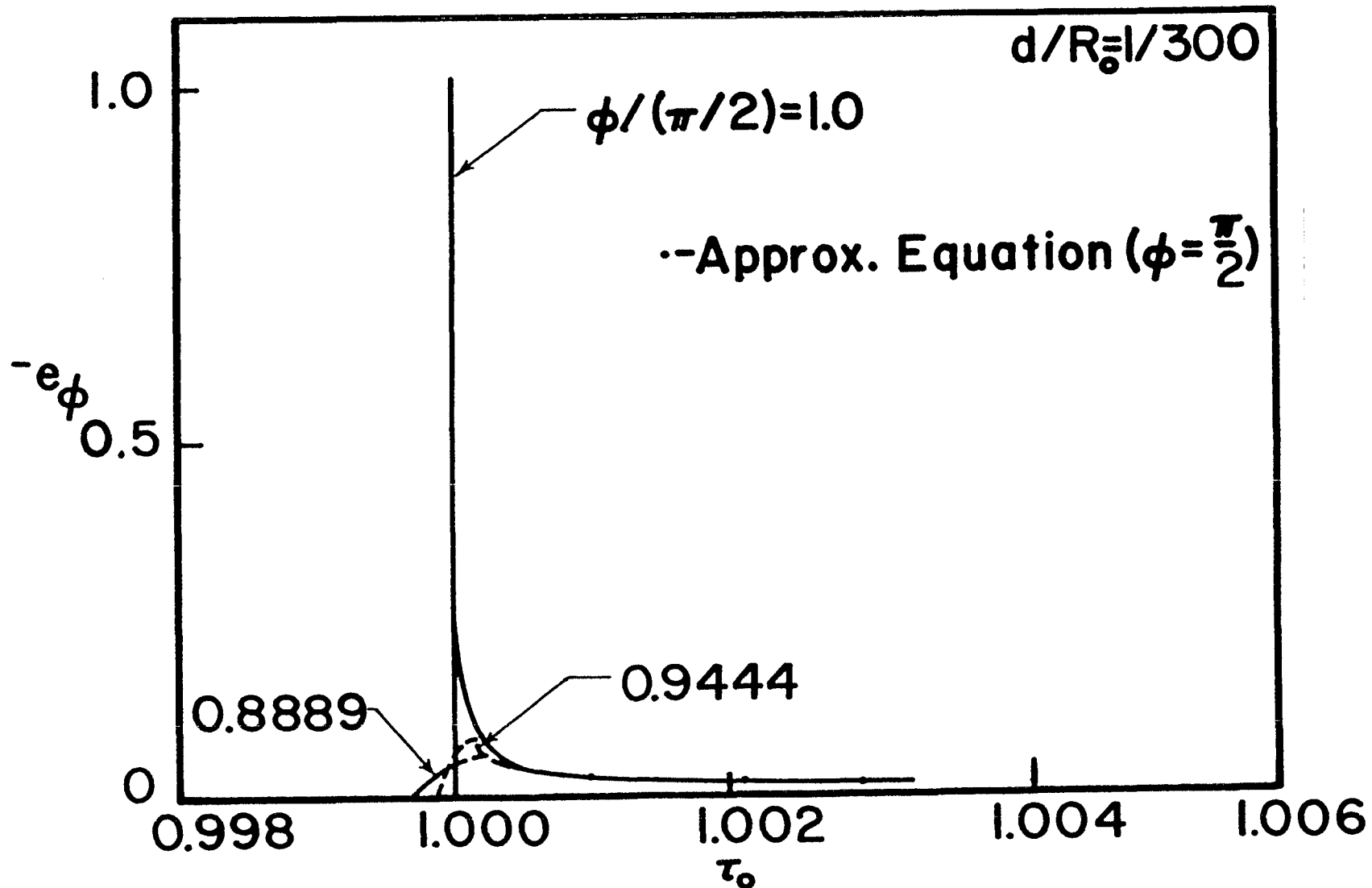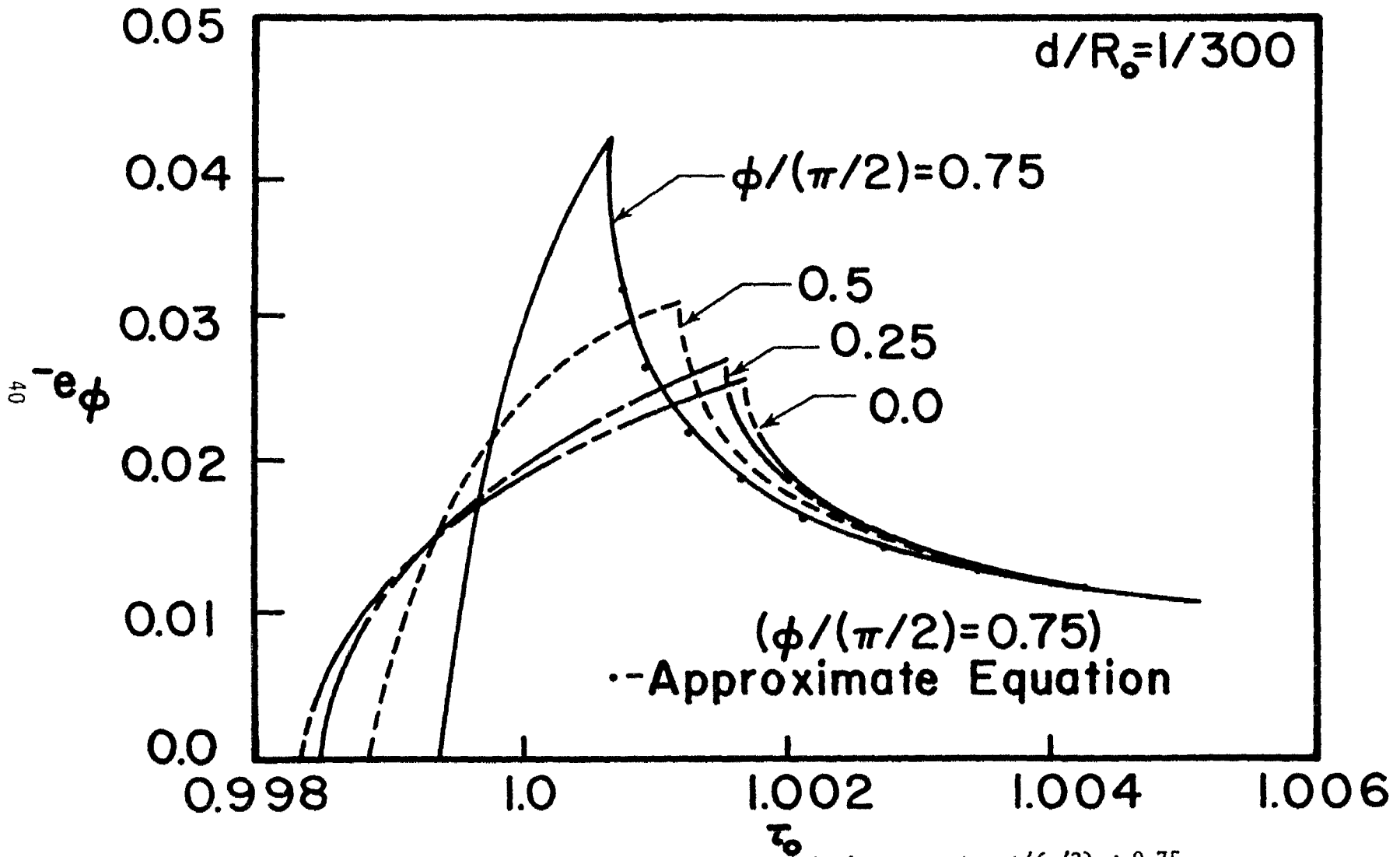Figure 14B. h_z vs. τ_0 with $d/R_0 = 1/300$ with the parameter $\phi/(\pi/2) \le 0.75$.
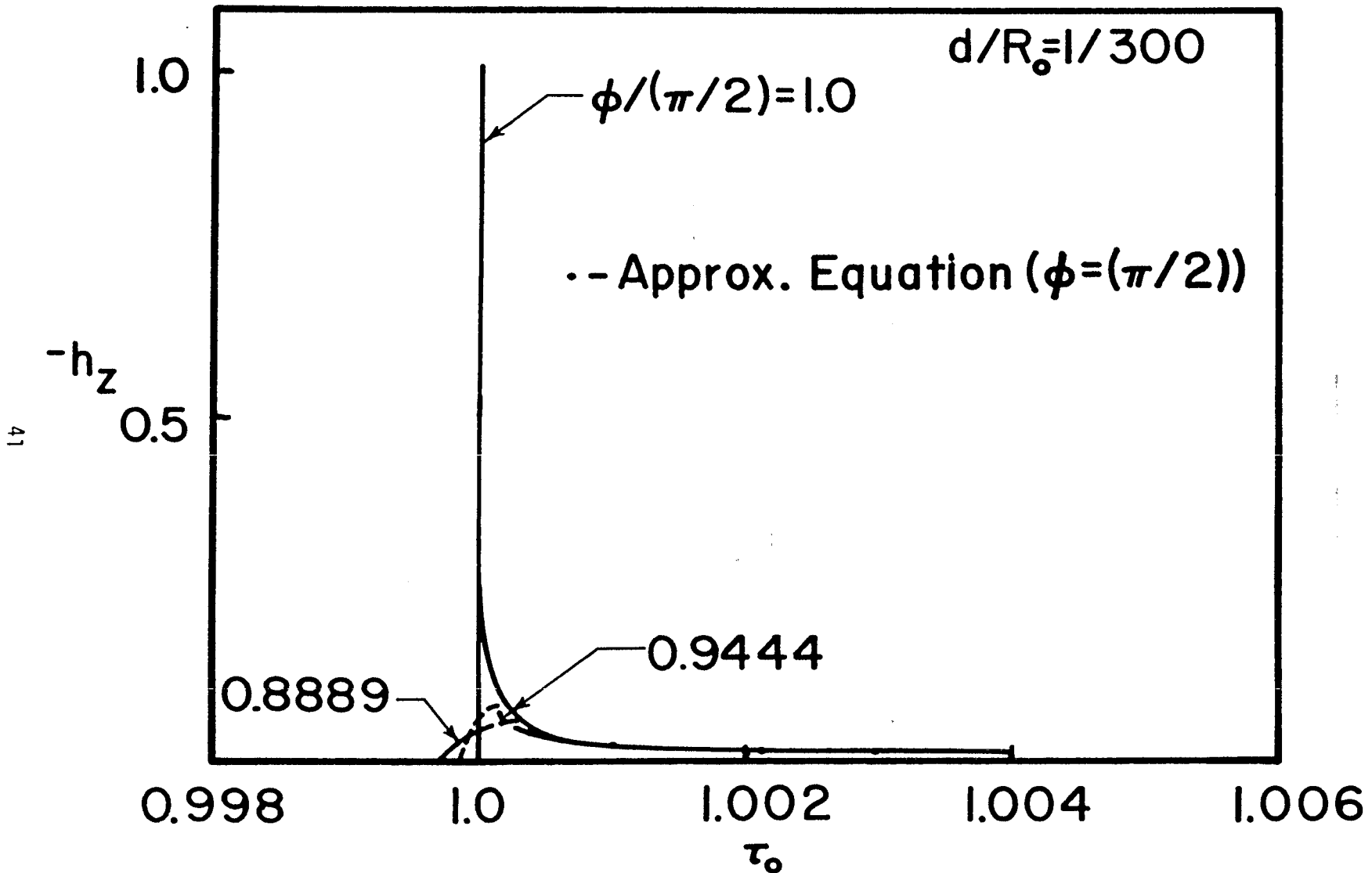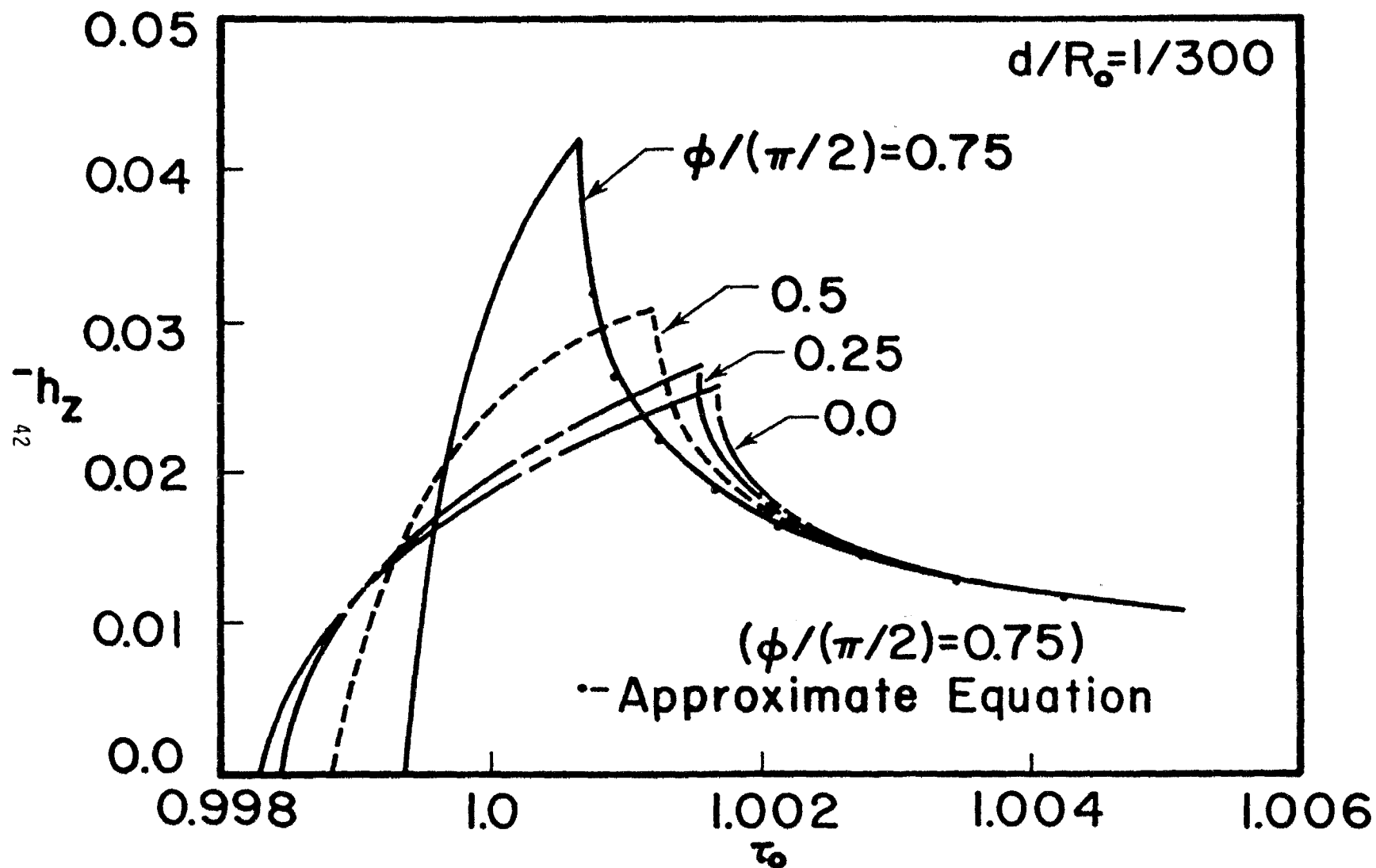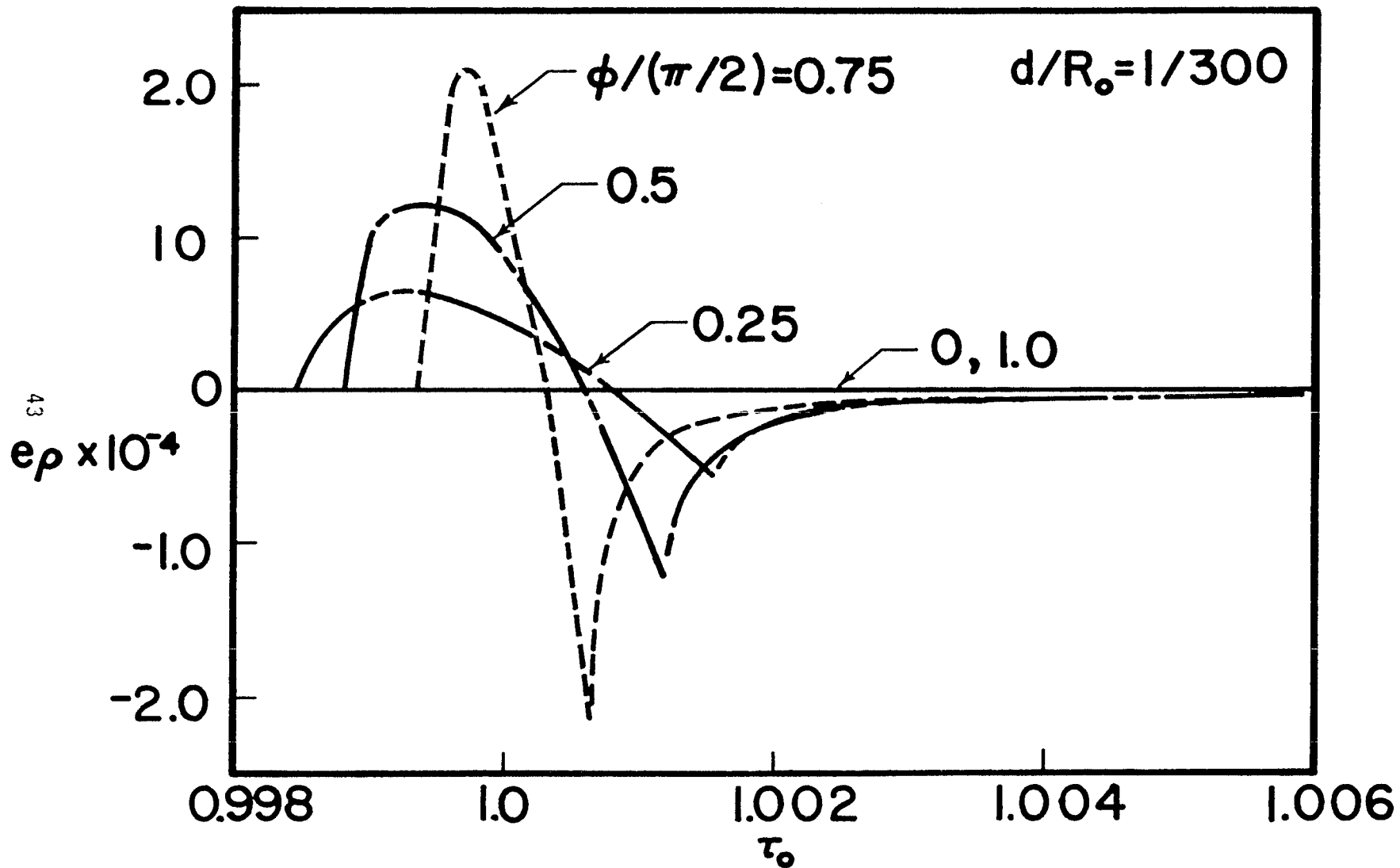
Figure 15. e_ρ vs. τ_0 for $d/R_0 = 1/300$ with ϕ as a parameter.

field component exhibits a finite rise-time characteristic followed by a decreasing magnitude as a function of time which rapidly approaches a limiting late-time behavior. Note that the peak of the functions occurs later in time and that the peak value decreases for decreasing values of $\phi/(\pi/2)$. This "spreading out" of the waveforms is a result of the time-delay experienced by the propagated waves from the slot as a function of angle which is related to the "dispersion effect" in the frequency domain. The computed transient behavior of the fields of equation (41) can be used to illustrate how the "spreading" or total rise-time of the waveform varies as a function of observation angle for the e_ϕ component of the single slot as shown in Figure 16. Again the curve emphasizes that the rise-time is dependent on angle of observation and that it changes most rapidly near broadside ($\phi=\pi/2$).

It is interesting to note that the numerical results of Figures 7A, 8A, and 10A indicate that the time response of a single strip has a short, but finite rise-time for $\phi/(\pi/2) = 1.0$ (i.e., broadside to the slot). This apparent rise-time is a result of the numerical convolution algorithm, and it can be shown that the actual time response has zero rise-time in this special case as inferred in Figure 16. From Figure 16, it is seen that the early time response for $\phi/(\pi/2)$ is determined for $1<\tau_0<(1+(d/2R_0)^2)^{1/2}$; thus, equation (45) reduces to the form,

$$ e_\phi \simeq -\frac{2}{\pi} \int_0^{\sqrt{a}} \frac{dx'}{(a-x'^2)^{1/2}} \tag{54} $$

where $a = (ct)^2 - R_0^2$ and $0<a^{1/2}< d/2$. This integral can be evaluated as

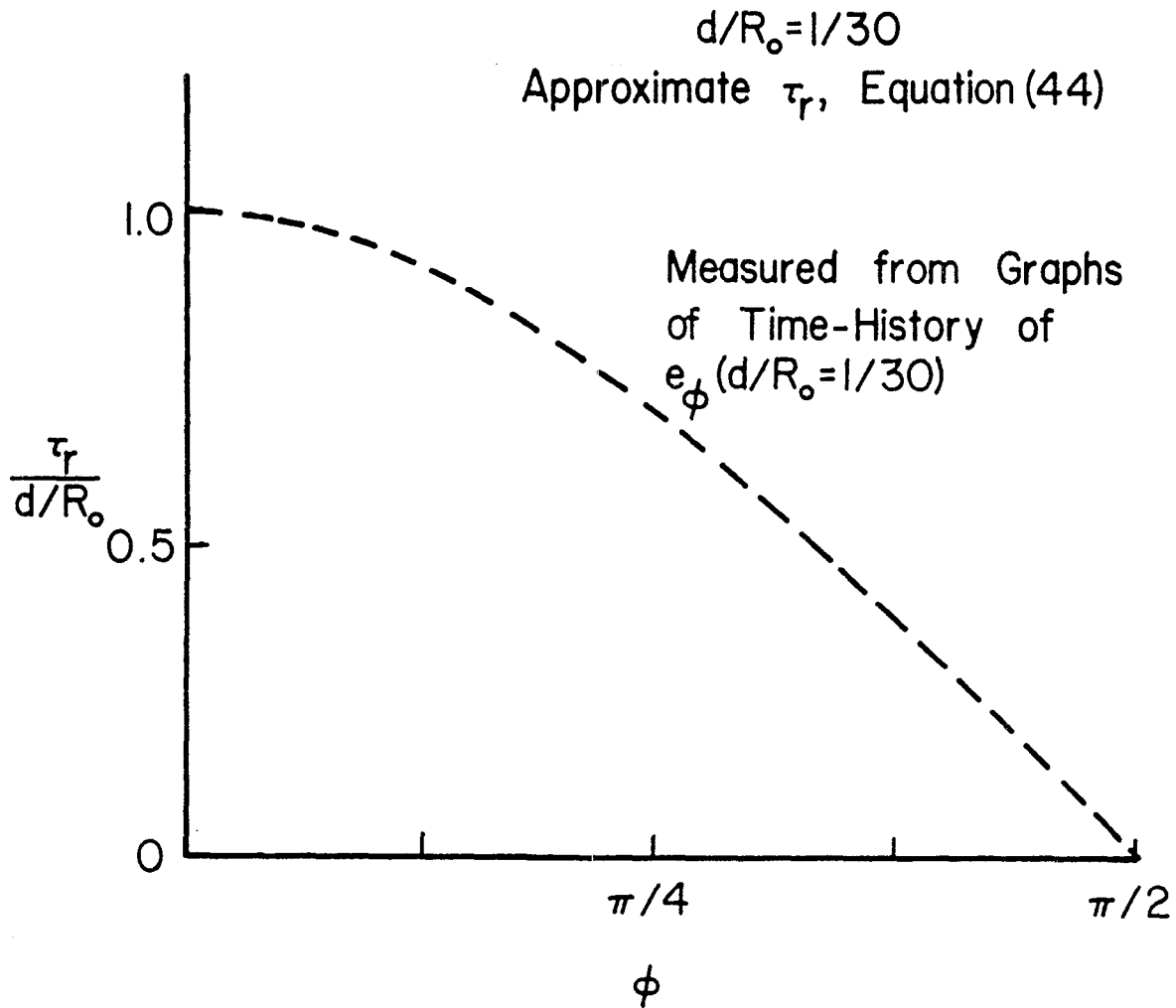$$ e_\phi = -\frac{2}{\pi} \int_0^1 \frac{d\mu}{\sqrt{1-\mu^2}} = -1 \tag{55} $$

44

Figure 16. Normalized rise-time as a function of angular position for e_ϕ component.

45

if the change of variables, $u=x'/\sqrt{a}$, is employed, and these results indicate that the normalized ϕ component of the electric field is independent of time during this interval where $\sqrt{a}$ is finite, however small, and less than $d/2$. Therefore, the time response for the special broadside case has zero rise-time and a constant magnitude until responses from all points on the slot have reached the observation point; then, the field decays in a manner described by equation (51).

It can be seen from Figure 7B that the approximate expression for the ϕ-component of electric field (equation 49) is in error for $\phi/(\pi/2)$ = 0.75 at d/R_0 = 1/5 while the h_z component of Figure 8B, as calculated with the approximate equation, is exact even for d/R_0 = 1/5. If the slot width-to-distance ratio is increased to 1/30, the e_ϕ components, calculated by both numerical and approximate expressions, are almost identical as shown in Figure 10B; and, if d/R_0 = 1/300, it is difficult to distinguish between the two computations as can be observed in Figure 13B. For $\phi/(\pi/2)=1$, it appears that the approximate equation is valid even at d/R_0 = 1/5 (See Figures 7A, 10A, and 11A) and that the accuracy of the approximation is a function of angular position as well as distance. The late-time behavior of the h_z component is exact in all cases as is evident from the graphs shown in Figures 8B, 11A, 14A, and 14B.

Thus, in summary, it has been shown with these results that the time-history of the far-field components of the planar slot is a critical function of both angular position and slot width-to-distance ratio. The e_ϕ and h_z components, which have the same basic shape, are distorted from the peaked broadside response for angles less than ninety degrees in both amplitude and shape.

With the results already obtained for the single slot in this investigation it is relatively easy to extend the theory, as well as the numerical procedure, to the array problem of Figure 1. Hence, if the surface equivalence theorem is applied to the N-element planar array of slots of Figure 17, then the composite magnetic current density can be expressed as

$$M_z(x,t) = 2\sum_{n=1}^{N} E_n(x') [u[x'-(x_n-d_n/2)] - u[x'-(x_n+d_n/2)]] \mu(t-\tau_n) \qquad (56)$$

where $E_n(x')$ is the electric field distribution on the nth slot, x_n is the distance to the center of the nth slot, τ_n is the "turn-on" time, and d_n is the width of the nth slot. Through the use of the magnetic current density of equation (56) and the theory developed in Section II, equations (36), (37), and (38) can be used to obtain integral expressions for the N-element slot array of the form (See Figure 17 for geometry)

$$E_\phi = 2\sum_{n=1}^{N} \int_{x_n-d/2}^{x_n+d/2} E_n(x') K_1[x,y,(t-\tau_n),x'] dx' \qquad (57)$$

$$E_\rho = -2\sum_{n=1}^{N} \int_{x_n-d/2}^{x_n+d/2} E_n(x') K_2[x,y,(t-\tau_n),x'] dx' \qquad (58)$$

and

$$H_z = -2\sum_{n=1}^{N} \int_{x_n-d/2}^{x_n+d/2} E_n(x') K_3[x,y,(t-\tau_n),x'] dx' \qquad (59)$$

where causality requires that $(t-\tau_n)>R/c$ for each individual term of the series expansion. The order of summation and integration has been interchanged in the formulation and the kernel expressions are the same functions

z is pointing out of the page

μ_o, ϵ_o

Magnetic Surface Currents Density Plus Image for all N-Elements

$-d_1/2$

0

y, y'

$d_1/2$

ϕ, ϕ

$x_2 - d_2/2$

x

$x_2 + d_2/2$

ρ, R_{01}

$x_n + d_n/2$

x_n

R_{on}

$x_n - d_n/2$

ϕ_n

(x, y)

$R = ((x - x')^2 + y^2)^{1/2}$

$= ((\rho \cos\phi - x)^2 + \rho^2 \sin\phi)^{1/2}$

$x_N - d_N/2$

x'

x_N

$x_N + d_N/2$

ϕ_N

$R_{on} = $ Distance from Center of the nth Slot to the field Point

$= ((x - x_n)^2 + y^2)^{1/2}$

$\phi = \tan^{-1}(y/x)$

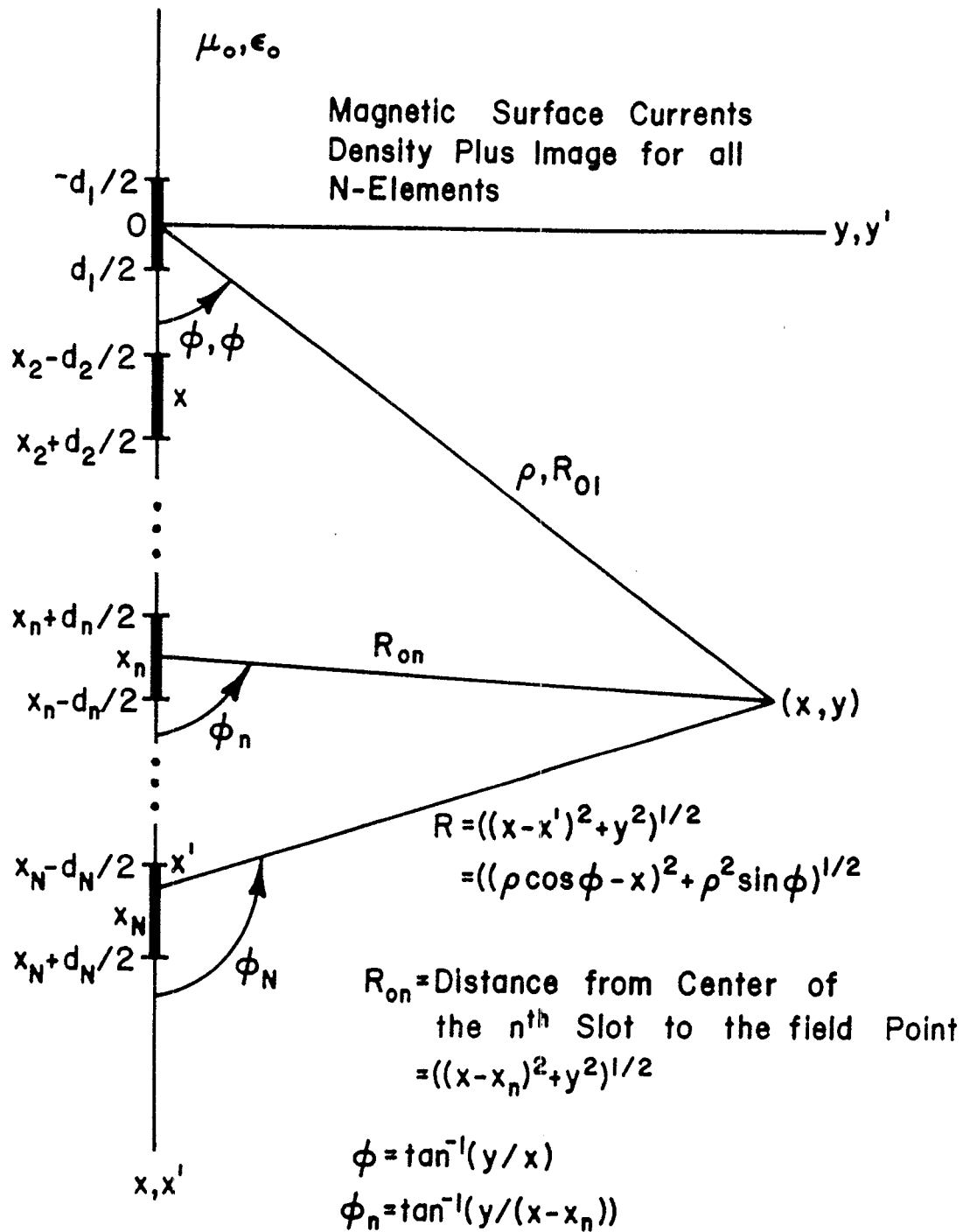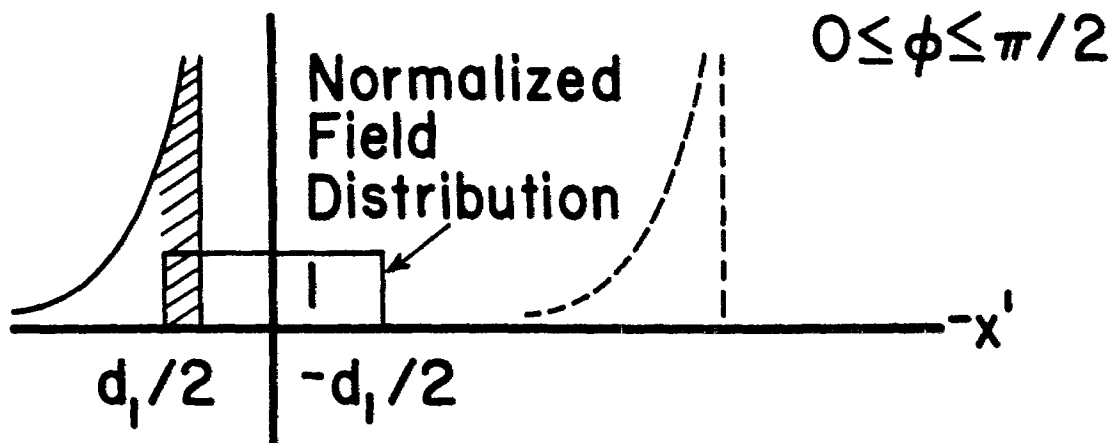$\phi_n = \tan^{-1}(y/(x - x_n))$

x, x'

Figure 17. Equivalent problem and coordinate system for a N-element planar array of two-dimensional slot sources.

defined in equations (30), (31), and (39) except that t is now replaced by $(t-\tau_n)$. These equations still represent exact expressions for the fields of this two-dimensional problem involving multiple slots.
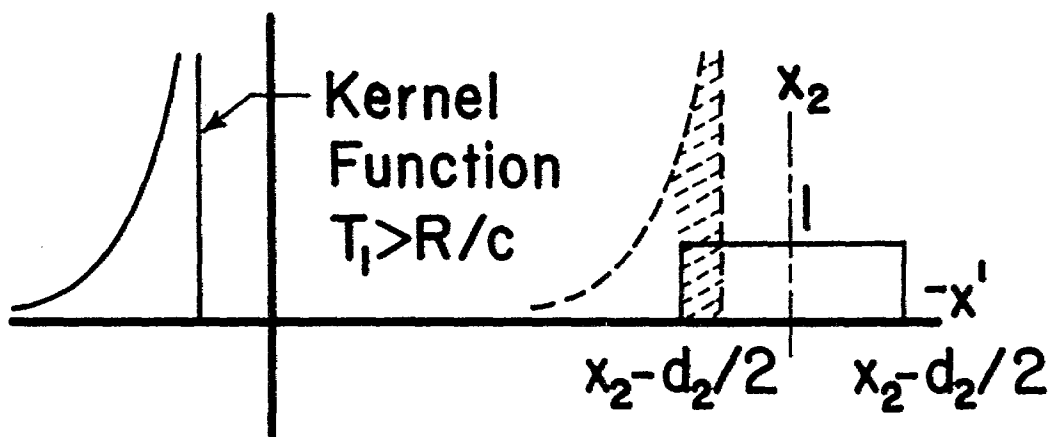
Thus, as can be seen from these expressions, the array problem simplifies to the summation of the transient responses of N single slots with the appropriate time delay and position. The individual transient response for each of these slots consists of a spatial-shifted convolution integral of the type investigated for the single slot which can include a time delay, τ_n. A graphical representation of the convolution integrals for the array is presented in Figure 18 for two times, T_1 and T_2, as a function of the spatial variable. As a result of the spatial distribution of the field distribution, it is easily seen that the sum of the individual integrals will consist of time-delayed responses of each array element. For a finite spacing between elements, the total response is not continuous as a result of the zero contribution between array elements; and, consequently, the time-history of the slot array is characterized by a "serrated" or sawtooth-type waveform. The shape of each serration of the response is a direct function of the position of the array element in relation to the observation point, and each separate contribution can be characterized by both the rise-time and delay of the response of a single element as a function of $\phi_n/(\pi/2)$. The time delay, t_d, between peaks of the serrations is a function of the spacing between edges of the array elements such that, from Figure 17,

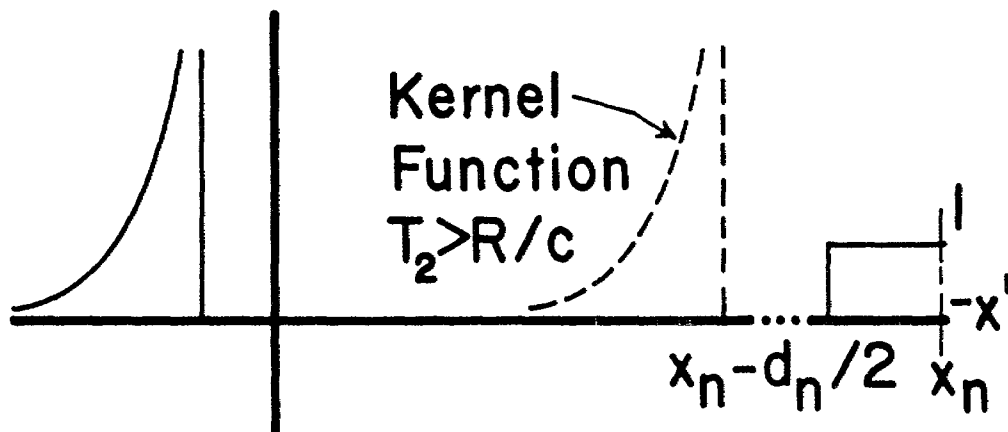$$\tau_{s_n} = t_s/(R_0/c) = (S_n - (d_n - d_{n-1})/2)\cos\phi_{n-1}/R_0 \qquad (60)$$

where τ_s is the normalized time delay, S_n is the center-to-center spacing of the nth and $(n-1)^{th}$ element. For an array of equally spaced, constant

49

$0 \leq \phi \leq \pi/2$

Normalized Field Distribution

$d_1/2$ $^-d_1/2$

$^-x'$

(A) Convolution for Slot No. 1

Kernel Function $T_1 > R/c$

x_2

$^-x'$

$x_2-d_2/2$ $x_2-d_2/2$

(B) Convolution for Slot No. 2

Kernel Function $T_2 > R/c$

$^-x'$

$x_n-d_n/2$ x_n

(C) Convolution for Slot No. n

Figure 18.   Graphical Representation of the Component field
integrals for an Array of Slot Sources.

50

width elements the time delay between response peaks becomes

$$\tau_s = S \cos\phi \tag{61}$$

in the far-field where S is the normalized element spacing, S_0/R_0, and S_0 is the actual element spacing. Thus, the slot array is completely characterized by the response of the individual array element, the spacing between elements, and the total number of the element which determines the aperture size and, therefore, the region of maximum response.

The expression for the ϕ-component of electric field of the N-element array (equation 57) has been solved using the numerical procedure utilized for the investigation of a single slot source. The results of this computer analysis for a two and a three-element array of equally spaced, constant-width elements are presented in Figures 19 and 20, respectively, for different element spacings. For S=1.0, i.e., all elements touching, the responses, with symmetrical placement of the array, are simply the transient response of a single slot element of either twice or three times the element source width for the appropriate array. This response consists of a unit magnitude, single pulse with zero rise-time and a long "fall-time" characteristic of the single slot responses of Figures 7, 8, and 10 for $\phi=\pi/2$. For S>1, the time-history of the total array consists of the sum of the time-delayed responses of each of the array elements. For the three-element array, the response separates from the S=1 case into a waveform having two peaks. One of these peaks is a response from the center slot and the other results from the remaining two symmetrically spaced elements which arrive at the same time. There is a striking difference between these contributions because the response from the center element is not drastically distorted because the time delay across this element is small and the time-
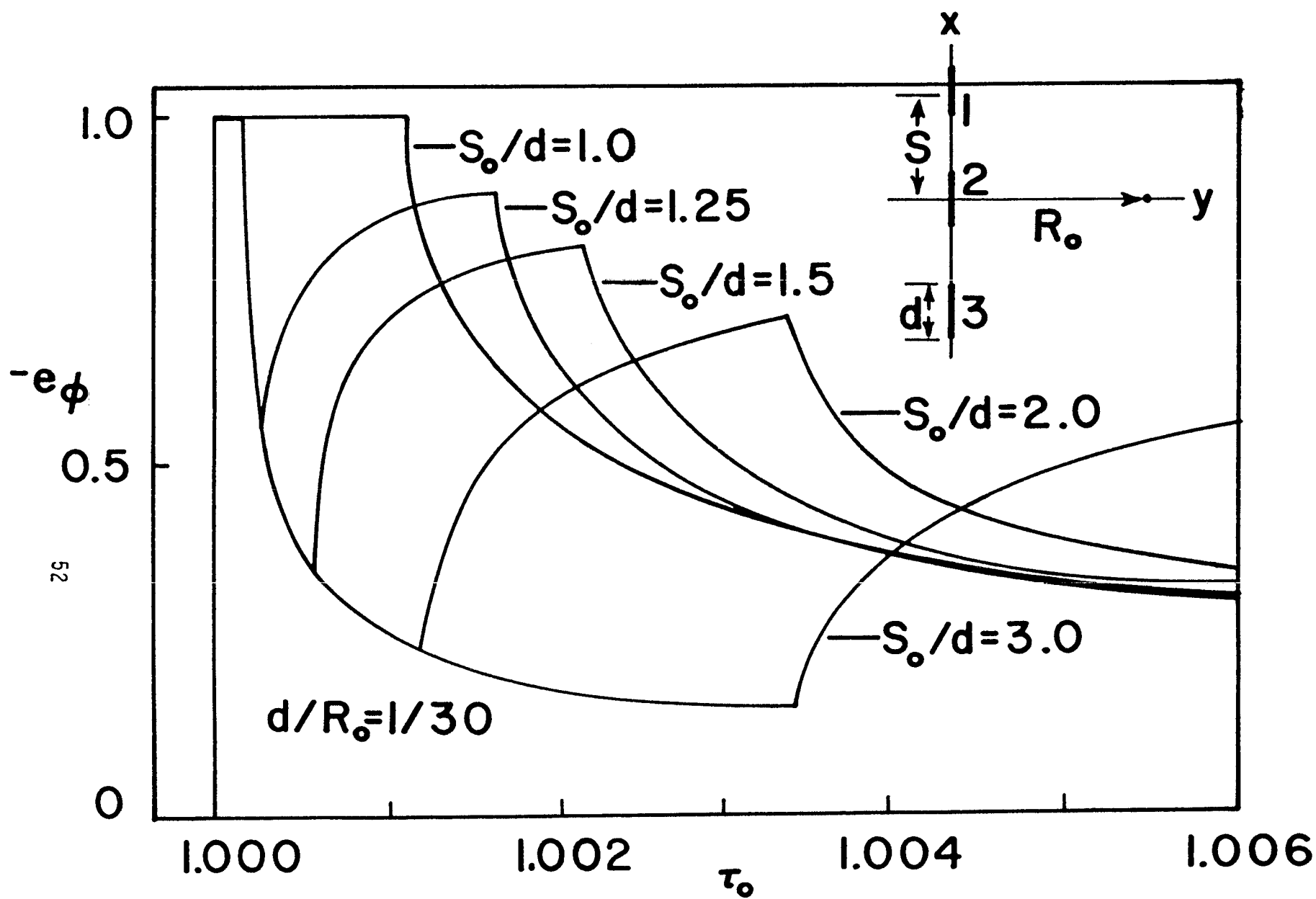
51

Figure 19. e_ϕ vs. τ_0 for a 3-Element Broadside Array of Slot Sources for Different Element Spacings.

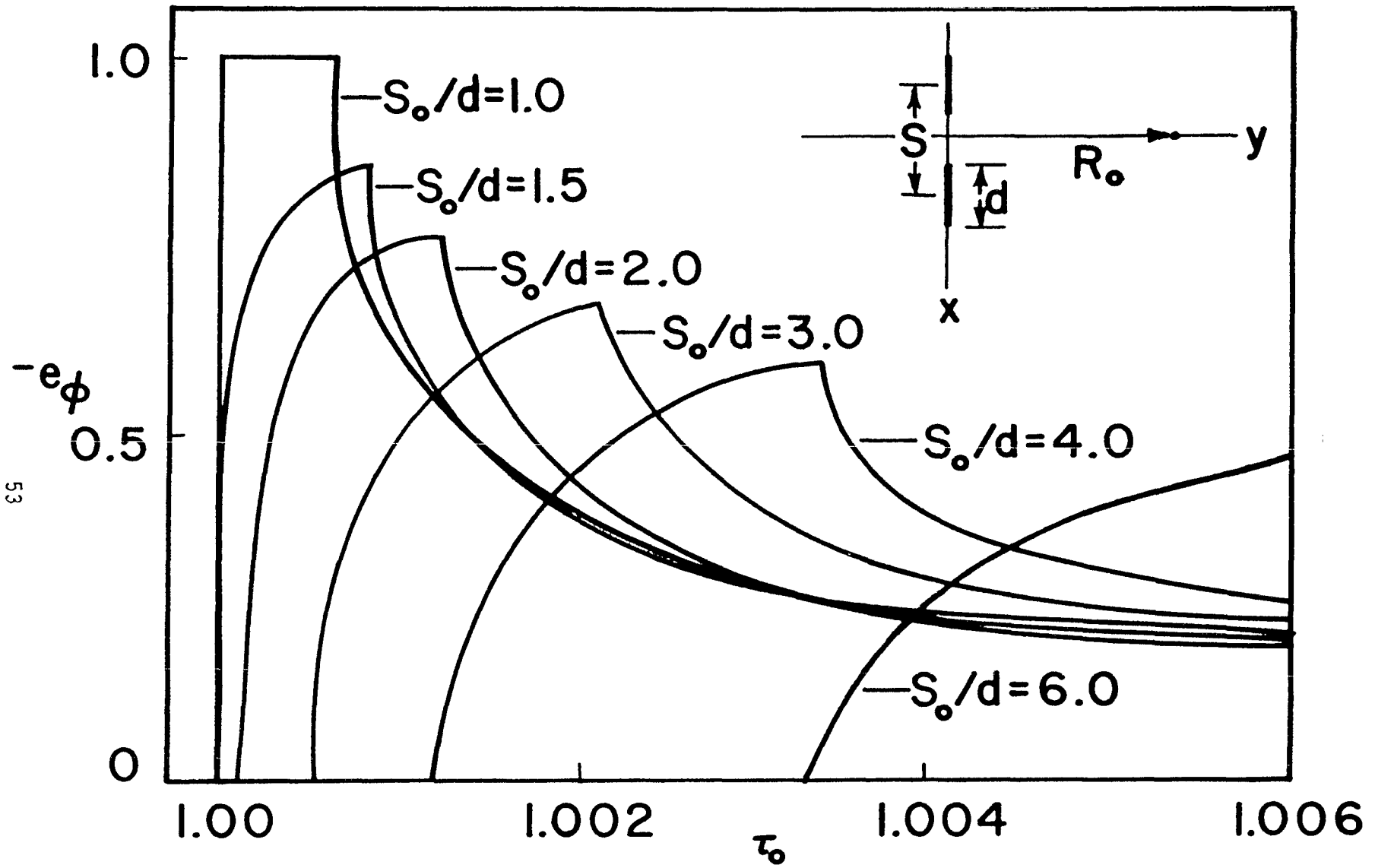Figure 20. e_ϕ vs. τ_0 for a 2-Element Broadside Array of Slot Sources for Different Element Spacings ($d/R_0 = 1/30$).

delay for points on the off-center elements increases as a function of position which results in deformation of the basic shape of the response. As shown in the other curves of Figure 19, the second peak is seen to decrease in both magnitude and width and to occur at later times for increases in element spacing. Numerical results for the two-element array are similar to that of the three element array without the first peak of the center element, as would be expected. The transient responses of 5, 7, and 9-element arrays of equally spaced, constant-width, slot sources is shown in Figures 21, 22, and 23, respectively, for $\phi(\pi/2)$ equal to 1 which shows that the array response is indeed the sum of the time-delayed response of each array element. In addition, the effects of changes in element spacing and element widths in a 9-element array are dramatized in Figures 24 and 25.
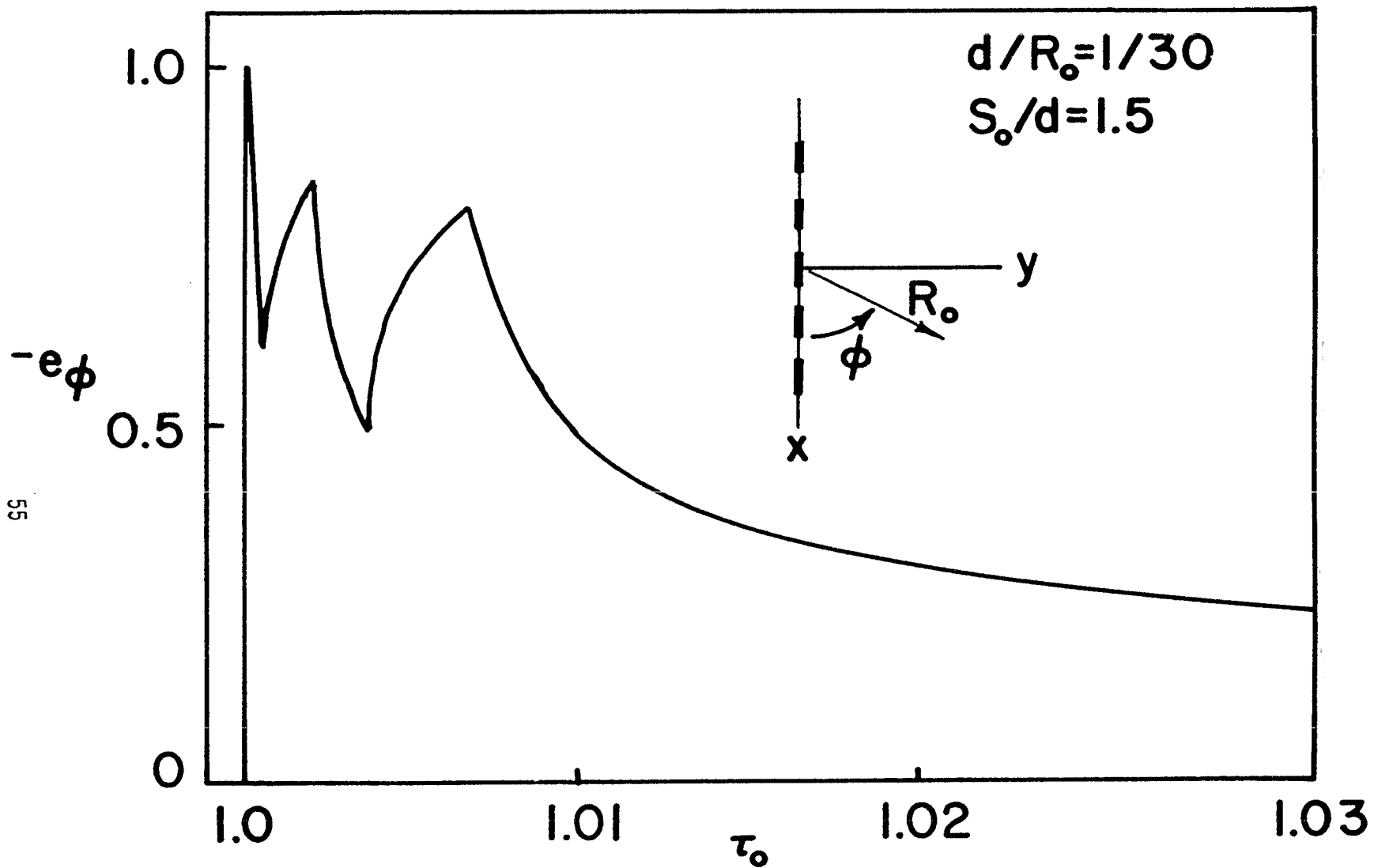
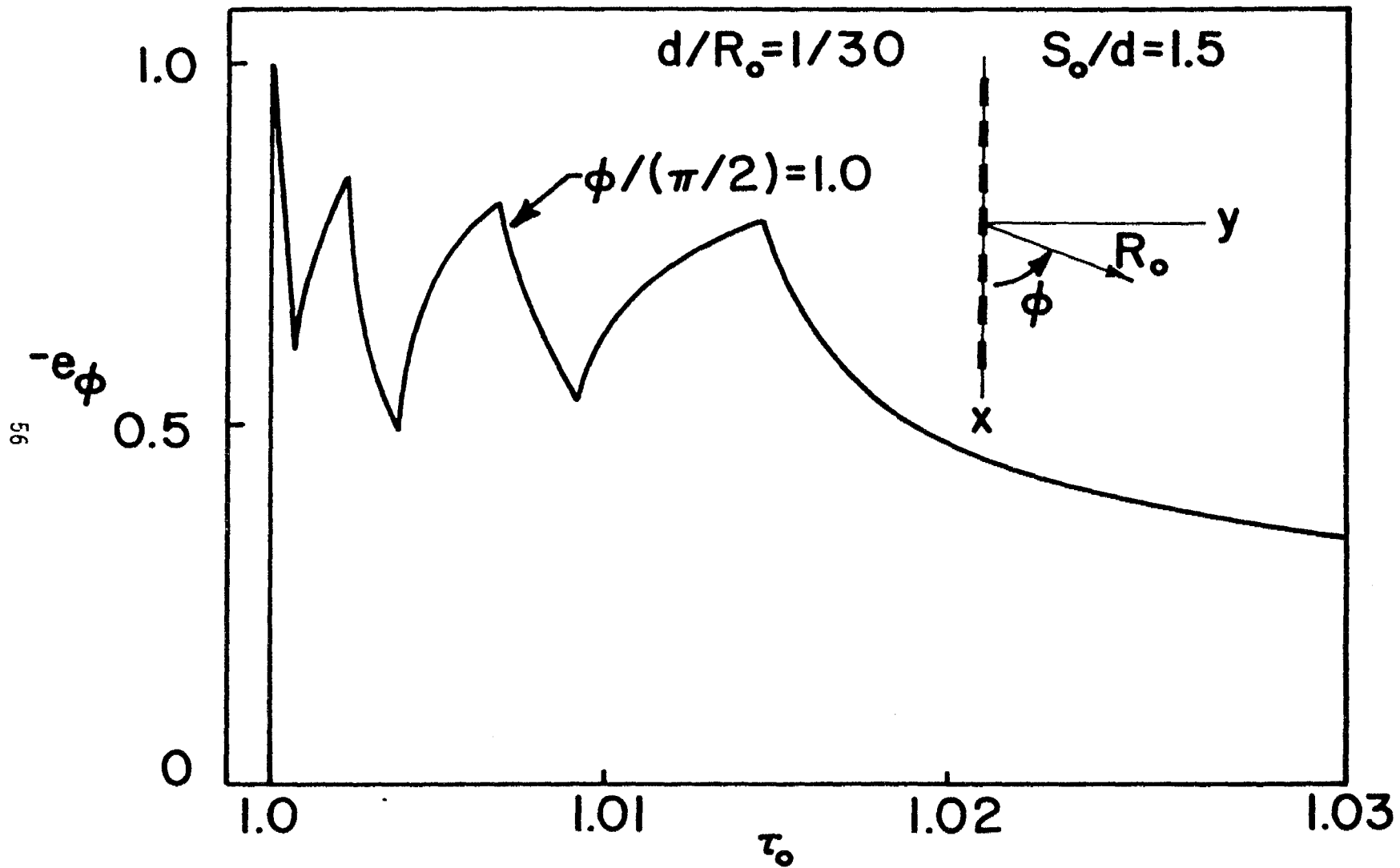Figure 21. e_ϕ vs. τ_0 for a 5-Element Array of Slot Sources as a Function of the parameter $\phi/(\pi/2)$.

Figure 22. e_ϕ vs. τ_0 for a 7-Element Array of Slot Sources as a Function of the parameter $\phi/(\pi/2)$.
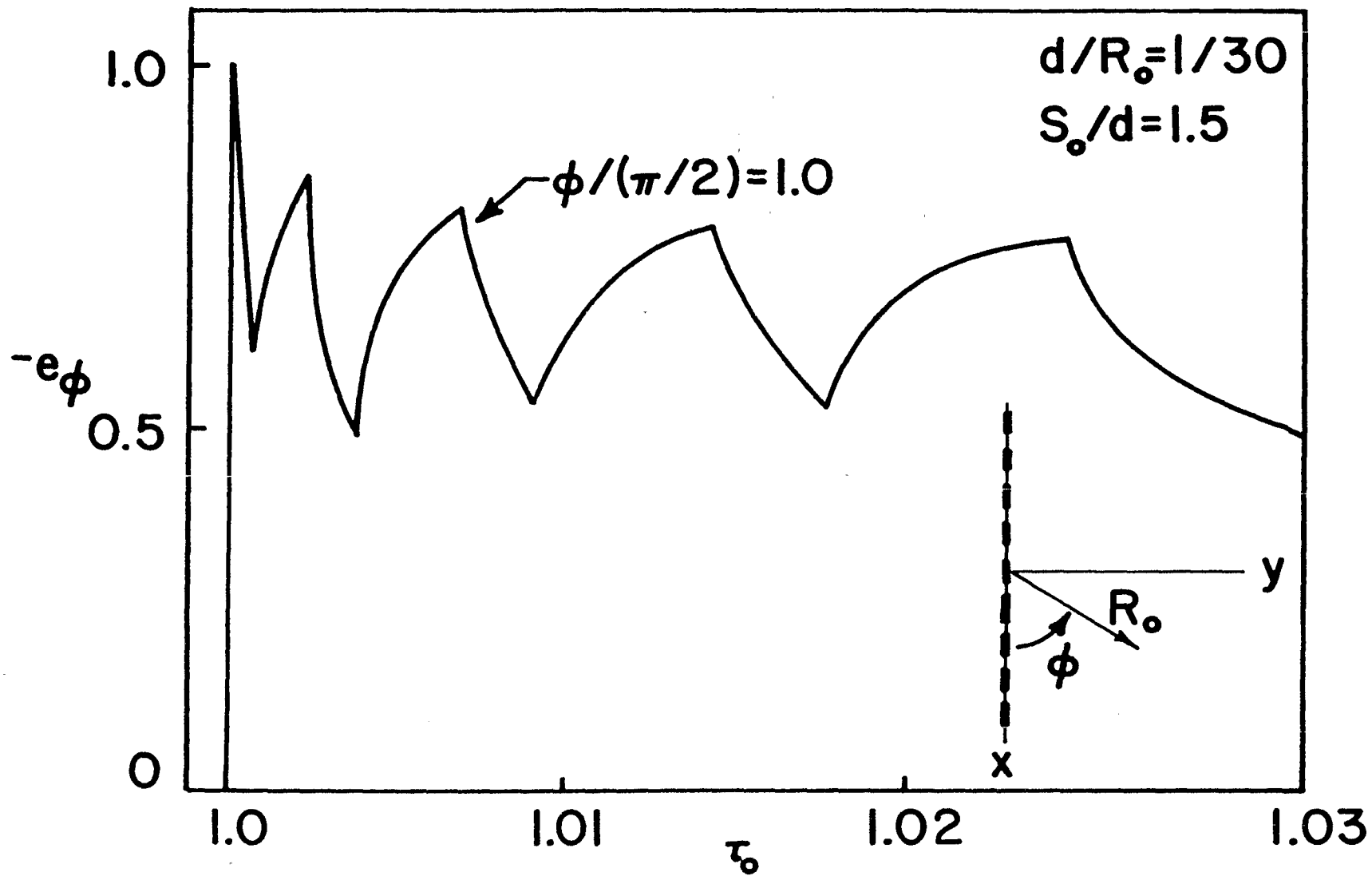
Figure 23. e_ϕ vs. τ_0 for a 9-Element Array of Slot Sources as a Function of the parameter $\phi/(\pi/2)$.
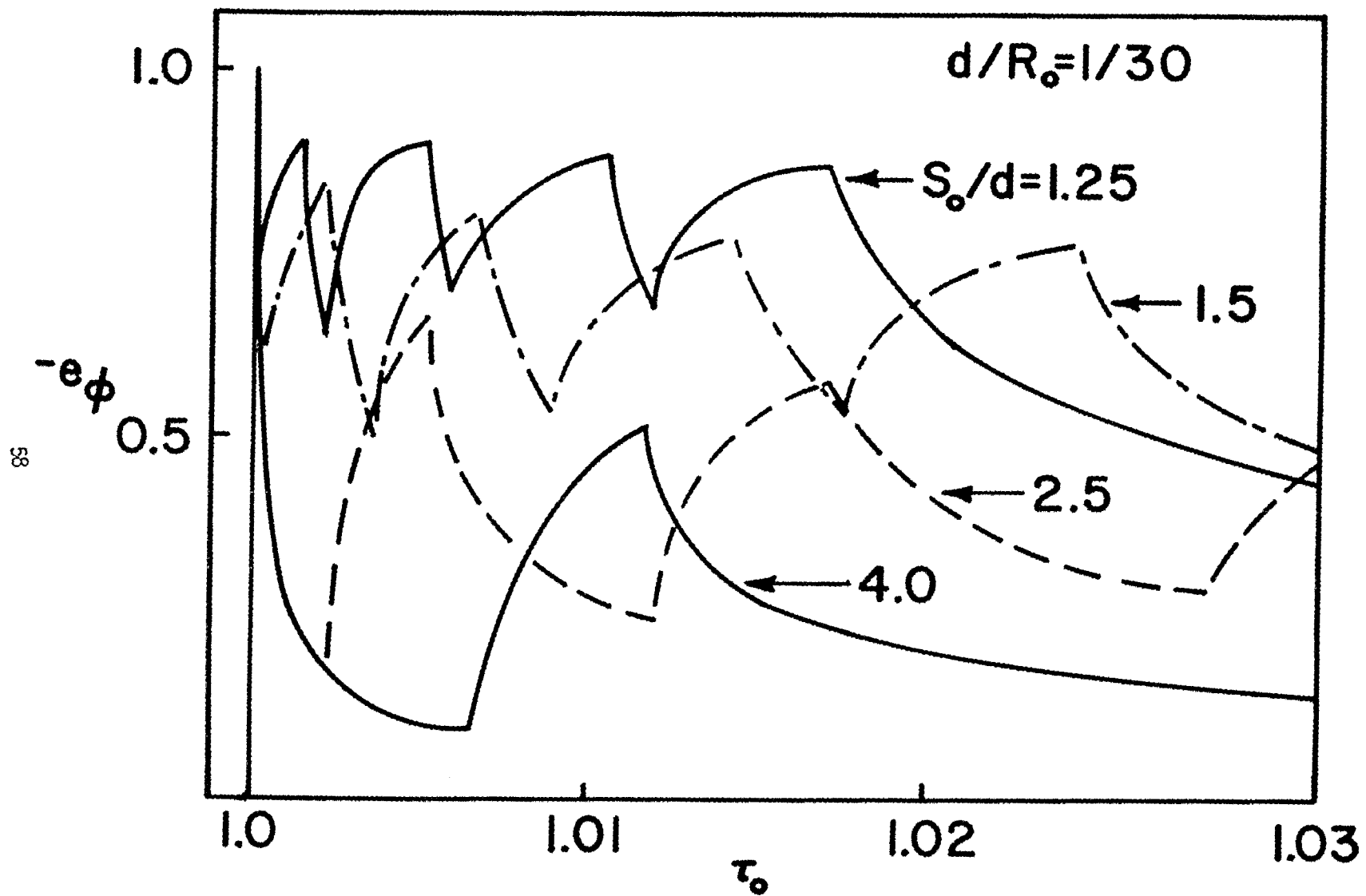
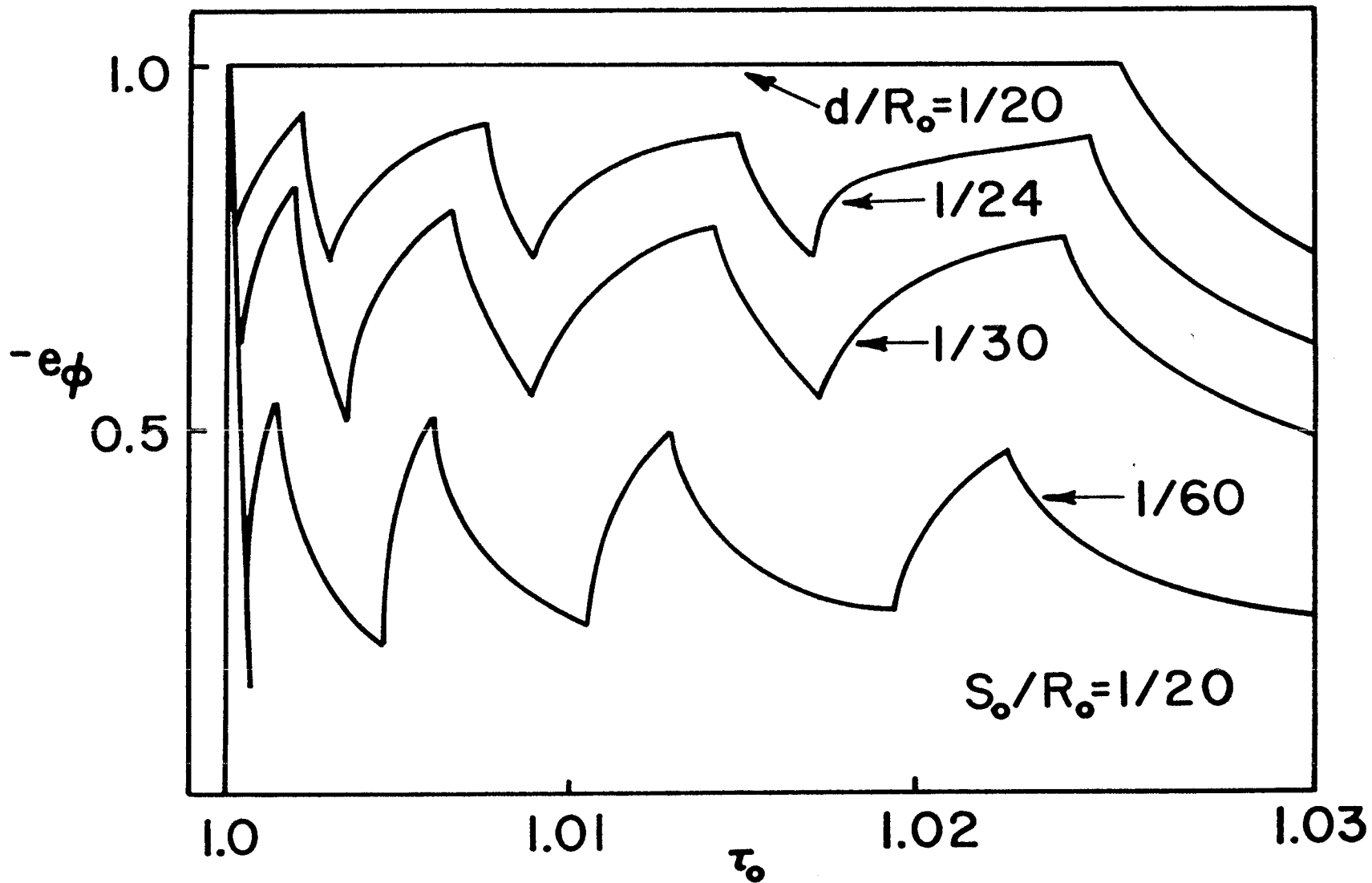Figure 24. e_ϕ vs. τ_0 for a 9-Element Array of Slot Sources for Different Element Spacings.

Figure 25. e_ϕ vs. τ_0 for a 9-Element Array of Slot Sources for Different Element Widths.

SECTION IV

CONCLUSIONS

This report presents general expressions for the transient radiated electric and magnetic fields for a planar array of sources with elements having known electric field distribution, as well as time delay, located on an infinite, perfectly conducting plane. The analysis of such arrays is based on the space-time Green's function approach to the electric vector potential problem rather than the more common frequency domain approach applied to related problems.[11]

Planar arrays of two-dimensional sources are analyzed using numerical computation of the appropriate superposition integrals in conjunction with related Green's function for constant amplitude distribution over the individual apertures. Plots of the time history of the radiated far-fields, as well as near fields, are presented for a single element and other array configurations for the constant amplitude distribution. Results of the field amplitude variation as a function of observation angle are presented for the single element. Note that the time history of an element is extremely sensitive to observation angle because of the time delay induced by the change in distance a given response must travel to reach the observation point.

The time history of the fields for these array elements is characteristic of the two-dimensional wave equation solution where the history consists of the response from the point on the element nearest the point of observation followed by responses which arrive later in time from points more distant on the infinitely long aperture. It is evident from the responses of the multielement arrays that the total response of the system is simply the linear superposition of the response of each element appropriately delayed in time for

60

the existing observation angle. In addition, from Figure 24, it can be observed that the time response at large distances from a finite array approaches the response of a single element for broadside observation because time delay to each element approaches zero.

REFERENCES

1. Carl E. Baum, "Some Characteristics of Planar Distributed Sources for Radiating Transient Pulses," Sensor and Simulation Note 100, Air Force Weapons Laboratory, Kirtland AFB, New Mexico, March 1970.

2. Carl E. Baum, "The Distributed Source for Launching Spherical Waves," Sensor and Simulation Note 84, Air Force Weapons Laboratory, Kirtland AFB, New Mexico, May 1969.

3. Carl E. Baum, Distributed Sources and Terminations for Launching and Terminating Plane Waves Either With or Without a Reflected Plane Wave," Sensor and Simulation 108, Air Force Weapons Laboratory, Kirtland AFB, New Mexico, May 1970.

4. Carl E. Baum, "General Principles for the Design of ATLAS I and II, Part I: ATLAS: Electromagnetic Design Considerations for Horizontal Versions," Sensor and Simulation Note 143, Air Force Weapons Laboratory, Kirtland AFB, New Mexico, January 1972.

5. Carl E. Baum, "General Principles for the Design of ATLAS I and II, Part IV: Additional Considerations for the Design of Pulser Arrays," Sensor and Simulation Note 146, Air Force Weapons Laboratory, Kirtland AFB, New Mexico, March 1972.

6. Carl E. Baum, "General Principles for the Design of ATLAS I and II, Part V: Some Approximate Figures of Merit for Comparing the Waveforms Launched by Imperfect Arrays onto TEM Transmission Lines," Sensor and Simulation Note 148, Air Force Weapons Laboratory, Kirtland AFB, New Mexico, May 1972.

7. R. F. Harrington, Time Harmonic Electromagnetic Fields: McGraw Hill Book Co., New York, 1961.

8. M. D. Greenberg, Application of Green's Functions in Science and Engineering: Prentice-Hall, Inc., Englewood Cliffs, N.J., 1971.

9. M. F. Garner and J. L. Barnes, Transients in Linear Systems: John Wiley and Sons, Inc., New York, 1942.

10. C. D. Hodgman, CRC Standard Mathematical Tables: .Chemical Rubber Company, Cleveland, Ohio, 1957.

11. Carl E. Baum, "A Simplified Two-Dimensional Model for Fields Above the Distributed-Source Surface Transmission Line," Sensor and Simulation Note 66, Air Force Weapons Laboratory, Kirtland AFB, New Mexico, December 1968.